GEO 511: Master Thesis

Creation of synthetic imaging spectroscopy time series from airborne and ground based spectral data

Fiona Utzinger
09-724-196

Supervisors:
Dr. Andreas Hüni
Anna Schweiger

Faculty Representative:
Prof. Dr. Michael E. Schaepman

Remote Sensing Laboratories
Department of Geography
University of Zurich

April 17, 2015

Abstract

Remote sensing provides spatial and temporal data based on satellite, aerial and in situ measurement systems and offers the possibility to get spatially continuous information about landscapes over large areas. As vegetation and its properties are dynamic, not only the current state of vegetation is of interest but also its development over time. Several time series from spaceborne broadband sensors exist but there is a lack of time series of high resolution airborne sensors. To enable vegetation monitoring over time this study combined airborne and in situ measured spectral data and traditional vegetation sampling to show vegetation development.

This master thesis was an explorative study that created two synthetic Airborne Prism Experiment (APEX) images based on one APEX image and Analytical Spectral Devices (ASD) measurements from three different months. The result is a time series of three APEX images: a synthetic image for June, the original one for July and another synthetic image for August 2013.

The conducted vicarious validation of the data disclosed many problems as atmospheric compensation problems for the APEX data, differences in the ASD reflectance factors between spatial clusters and measurements dates, outliers in the ASD data and high scattering in the white reference measurements.

Time transformation functions were generated but it was not possible to link the changes over time to the cover ratio of vegetation and soil. Two synthetic APEX images were created but as their validation was not sufficient, they have to be used with caution.

For further work the sampling design has to be well elaborated, contain more plots than this study and cover the entire range of vegetation types and possible influence factors on the vegetation development in the study area.

Contents

List of Figures

List of Tables

Abbreviations

ASD	**A**nalytical **S**pectral **D**evice
APEX	**A**irborne **P**rism **EX**periment
CV	**C**ross **V**alidation
DEM	**D**igital **E**levation **M**odel
ESA	**E**uropean **S**pace **A**gency
EVI	**E**nhanced **V**egetation **I**ndex
FOV	**F**ield **O**f **V**iew
LAI	**L**eaf **A**rea **I**ndex
LOO-CV	**L**eave **O**ne **O**ut **C**ross **V**alidation
LSU	**L**inear **S**pectral **U**nmixing
NDVI	**N**ormalized **D**ifference **V**egetation **I**ndex
NIR	**N**ear **I**nfra **R**ed
ROI	**R**egion **O**f **I**nterest
RSL	**R**emote **S**ensing **L**aboratories
SNP	**S**wiss **N**ational **P**ark
SWIR	**S**hort **W**ave **I**nfra **R**ed
TTF	**T**ime **T**ransformation **F**unction
TV	**T**ransformation **V**ector
VCR	**V**egetation **C**over **R**atio
VV	**V**icarious **V**alidation
WR	**W**hite **R**eference

Chapter 1

Introduction

1.1 Motivation

Grassland ecosystems are spatially and temporally heterogeneous landscape elements (Schweiger et al., 2014) and represent one of the largest landscape units in the terrestrial system, thus they play an essential part in the global biodiversity (Schuster et al., 2015). Monitoring and modelling grassland characteristics and changes are critical to understand important processes such as biodiversity change and carbon sequestration (Li et al., 2013b) moreover their variability in time and space helps to understand wildlife behaviour (Schweiger et al., 2014).

Direct measurements in grasslands are time consuming and expensive since they require extensive field work (Psomas et al., 2007). Remote sensing provides spatial and temporal data based on satellite, aerial and in situ measurement systems (Muchoney, 2008) and offers the possibility to get spatially continuous information about landscapes over large areas (Kerr and Ostrovsky, 2003). These data allow to efficiently monitor the current status of ecosystems (Kneubühler et al., 2014) and to derive biophysical parameters over large areas (Psomas et al., 2007).

Spectral vegetation indices have been widely used to retrieve biophysical parameters for over three decades (Vescovo and Gianelle, 2008). Most of them are calculated as ratios or normalized differences from near infra red (NIR) and visible bands. Biomass (e.g. NDVI; Rouse et al. (1974)), vegetation cover (e.g. SAVI; Huete (1988)) and vegetation water content (NDWI; Hardisky et al. (1983); Gao (1996)) are some examples of vegetation characteristics that can be derived from spectral data. Remote sensing also

offers the possibility to assess the quality of vegetation for example by deriving nitrogen or phosphorous concentration using continuum-removed absorption features (Mutanga et al., 2004).

The Airborne Prism Experiment (APEX; Schaepman et al. (2015)) is an airborne imaging spectrometer of the European Space Agency (ESA) developed by a Swiss-Belgium consortium and entered its operational phase in 2010 (Hueni et al., 2012). With its wavelength coverage from 380 to 2500nm (Jehle et al., 2010) and its pixel size of 1.5 to 2.5m (Hueni et al., 2012), APEX is suitable for the deviation of biophysical parameters at high spatial resolution. In the last years APEX data was for example used to determine the ecosystems total surface water content (Kneubühler et al., 2014), sun-induced chlorophyll fluorescence (Damm et al., 2015), nitrogen content (Schweiger et al., 2015) or to predict fresh above ground biomass (Schweiger et al., 2014).

Vegetation analyses can also be based on spectral in situ measurements. In the field, hand held spectroradiometers, such as the Analytical Spectral Device (ASD (ASD Inc., Boulder, CO, USA)), are used to acquire spectral data with a high spectral resolution. Pullanagari et al. (2011) stated that in situ measured canopy reflectance can be used to predict pasture quality in a timely fashion, assisting farmers in their decision making. Sha et al. (2012) correlated NDVI values based on spectral field measurements with different grazing intensities and Chen et al. (2009) predicted above ground biomass of alpine meadows. Rahman and Gamon (2004) were able to differentiate and characterise burned and unburned grassland based on in situ spectral measurements sampled along transects at three different times after a fire event. Acquiring spectral field measurements is time expansive, but delivers reasonable results for analysis in limited study areas. Spectroradiometers can also be used to complement airborne or spaceborne data, for example by collecting endmembers for spectral unmixing (Kneubuehler et al., 1998) or measuring spectral reflectance of a bright surface for vicarious calibration of airborne or spaceborne data (Kneubühler et al., 2003).

1.2 Data combination

The combination of remotely sensed data with other kinds of data can offer new possibilities and can improve the monitoring of vegetation parameters for answering ecological questions (Lawley et al., 2015). Spectral data can be combined with different kinds of

data, e.g. meteorological data or biomass measurements. Pottier et al. (2014) derived topographic variables like elevation, slope and aspect from a digital elevation model and combined these with airborne imaging spectrometer data to predict alpine plant species distribution. For validation they used species cover estimated in the field. Ramoelo et al. (2013) demonstrated the importance of an integrated modelling approach by estimating grass quality based on spectral field measurements, nitrogen and phosphorus concentration analyses and environmental variables as climate, soil and topography.

There also exists the possibility to combine different kinds of spectral measurements but some requirements have to be fulfilled. The spectral resolution has to be the same. If this is not the case, the higher resolved data have to be resampled. The same holds for the spatial resolution, whereat the higher resolved data has to be resampled. There are several studies where field spectrometer measurements were combined with airborne or spaceborne data and with biomass measurements (e.g. Boschetti et al. (2007); Psomas et al. (2007); Numata et al. (2008); Demircan and Mauser (1994)). Boschetti et al. (2007) and Psomas et al. (2007) developed biomass models based on field spectrometer data and biomass measurements and performed an upscaling by applying the models to the spaceborne image. Both resampled the spectrally higher resolved field data based on the central wavelengths and band width of the spaceborne data. Psomas et al. (2007) did not take further steps to analyse the match between the data, whereas Boschetti et al. (2007) calibrated the spaceborne data with respect to the field data. The preparation steps conducted before combining different kinds of data differ and are dependent on the data type. Lawley et al. (2015) see a growing demand for combination of in situ measurements and airborne or spaceborne data for mapping and monitoring vegetation condition across a range of scales.

This study is about the combination of airborne and field based spectral data and includes a temporal component as vegetation changes over time.

1.3 Time series

As vegetation and its properties are dynamic, not only the current state of vegetation is of interest but also its development over time. Intra-annual time series enable to observe vegetation's phenological differences and help classifying small scale vegetation types (Schuster et al., 2015). The key issue for this kind of applications is the availability of a

constant spatial and seasonal coverage (Esch et al., 2014).

Some earth observation satellites are in the orbit since many years and some were replaced several times by a sequel satellite in the last decades. The data of the Landsat series of satellites constitutes the longest record of the Earth's surface seen from space (Bryant et al., 2002). This provides the possibility to track changes of the vegetation over multiple decades (Lymburner et al., 2013).

Satellites that cover the entire earth in several days provide data to observe not only annual but also seasonal changes. The revisit time of Landsat of 16 days can be problematic, if at the time of image acquisition the site of interest is covered by clouds (Li et al., 2013a).

Airborne imaging spectrometers are more flexible in assigning the time steps of the time series and often provide higher spatial and spectral resolution than spaceborne sensors. But flight campaigns have to be well planned and they are expensive.

Several time series from spaceborne broadband sensors exist but there is a lack of time series of high resolution airborne sensors. To enable vegetation monitoring over time, even if there is only one high resolution airborne image, the idea to create synthetic time series based on airborne and ground based data was developed.

1.4 Goal and Hypotheses

This thesis was based on two of the previously introduced topics: the combination of differently originated data and time series. Different kinds of spectral data were combined, not to improve vegetation analyses primilary, but rather to fill the lack of airborne time series. This thesis combined airborne and in situ measured spectral data and traditional vegetation sampling to show vegetation development. The vegetation changes were linked to the cover ratio of vegetation and soil as only the vegetation, but not the soil, changes between the months.

The goal of this master thesis was to create two synthetic Airborne Prism Experiment (APEX) images based on one APEX image and Analytical Spectral Devices (ASD) measurements from three different months. The result is a time series of three APEX images: a synthetic image for June, the original one for July and another synthetic image for August 2013. The synthetic images were validated using vegetation data collected in the field.

Four hypotheses were formulated for this study. They demand different methodologies but build up on each other and contribute to the goal of this master thesis.

I. The cover ratio of vegetation and soil of the alpine grassland can be determined using Linear Spectral Unmixing (LSU).

II. For each wavelength a transformation vector (TV) consisting of a proportional linear gain and a proportional offset can be identified to transform ASD spectra to APEX equivalent spectra or vice versa.

III. The change in spectral behaviour over time is proportional to the vegetation cover ratio.

IV. The combination of airborne and ground based spectral data allows creating synthetic spectral time series.

1.5 Organization of this thesis

In the next Chapter, the study area and data are presented and data preprocessing, mainly based on a vicarious validation (VV), is explained. Furthermore, the time transformation of the APEX image and the creation of the two synthetic images is described. The third Chapter presents the results of the preprocessing steps and the validation of the synthetic APEX images (APEX') based on an NDVI-biomass model.
In the next Chapter the differences, similarities and dependencies of the field based ASD data and the airborne APEX data are discussed, as well as the process leading to the synthetic images.
In the final Chapter the important findings are summarised and recommendations for further work are presented.

Chapter 2

Material & Methods

2.1 Study Area

The study was conducted in the Swiss National Park (SNP), located in the southeast of Switzerland. The SNP covers an area of 170km^2 whereof about half of the area is covered by vegetation, mainly forests and alpine grassland. The elevation ranges from 1400 to 3170 m above sea level and the plant growing season lasts from mid-May until mid-September (Schweiger et al., 2014).

The study area is located in the upper part of Val Trupchun, a southeast- to northwest-orientated valley in the southwest of the SNP with an area of 22km^2. The predominant land cover types in Val Trupchun are alpine grassland communities, rocks (manly limestone and calcareous schist), bare soil, open forest stands and snowfields, depending on the season. The grassland communities in the SNP are heterogeneous due to small-scale micro-relief variability caused by variations in microclimate and soil properties (Schweiger et al., 2014). Figure 2.1 shows a view towards the end of Val Trupchun.

Different parts of Val Trupchun were included in the SNP in 1912, 1932 and 1961 and have not been managed since then. The only human interactions are due to touristic activities, although visitors are requested to stay on path. The grassland gets grazed by populations of red deer, chamois and ibex.

FIGURE 2.1: Photo towards the end of Val Trupchun from July 12, 2013.

2.2 Data

2.2.1 APEX Imaging Spectrometer Data

The Airborne Prism Experiment (APEX, Schaepman et al. (2015)) is an airborne imaging spectrometer of the European Space Agency (ESA) developed by a Swiss-Belgium consortium and entered its operational phase in 2010 (Hueni et al., 2013b). APEX measures the solar reflected radiance in the wavelength range from 380 to 2500 nm with up to 330 reconfigurable spectral bands (Jehle et al., 2010). The pushbroom scanner covers a field of view of 28° and records 1000 spatial across track pixels with a ground pixel size of 1.5 to 2.5 m depending on the flight altitude (Hueni et al., 2012).

The APEX data set used for this study was part of a flight strip collected over the SNP on July 12, 2013. The flight strip got recorded from 13.52 to 13.58 o'clock, about thirty minutes after solar culmination at 13.26 o'clock. The airplane flew from ENE to WSW on an average flight level of 6715 m above sea level.

The APEX data was geometrically and atmospherically corrected by the Remote Sensing Laboratories (RSL), University of Zürich (UZH). The APEX Processing and Archiving

Facility is the combined software and hardware designed to generate calibrated level 1 at-sensor radiances from APEX raw image streams (Hueni et al., 2009a). Calibration coefficients for the radiometric, geometric and spectral calibration were generated from system calibrations at the APEX Calibration Home Base (CHB) at DLR Oberpfaffenhofen (Gege et al., 2009). These CHB data were stored and processed within the APEX Calibration Information System (CAL IS), producing the so-called calibration cubes holding coefficients for each spatio-spectral pixel (Hueni et al., 2013a). All data were calibrated using calibration coefficients obtained in May 2013. Level 2 processing is based on PARGE for the geometric correction and ATCOR for the atmospheric correction (Schläpfer and Richter (2002); Richter and Schläpfer (2002); Richter et al. (2011)). The pixel size was resampled to 2 m and the spectral bands were resampled to 284 bands betweend 400 and 2420 nm. The geometric misregistration measured less than one pixel (± 2 m) in flat terrain and up to two pixels (± 4 m) on steep slopes (Damm et al., 2012). The subset taken of the flight strip measured 1720 x 1539 pixels and excluded the parts of Val Trupchun with only non vegetative surface such as rocks and snow. Figure 2.2 shows a true colour image of the APEX data used for this study.

2.2.2 Field measurements

Since 2010, 100 ground reference plots were established in Val Trupchun, whereof 78 plots are located inside the study area. These plots are homogeneous in themselves and represent the heterogeneity of the alpine grassland. They cover the entire range of exposure, elevation, expected range of grassland biomass, plant species composition and grazing intensity. They got established in an area of at least 50 x 50 m of grassland. An individual plot measured 6 x 6 m and was homogenous in species composition. Plots did not contain large objects such as trees, rocks or trails and were located at least 6 m from such objects. The minimum distance between plots measured 20 m. All plots were geo-located, using a high-precision GNSS (Global Navigation Satellite System) receiver (Leica 1200+, Leica Geosystems, Heerbrugg, Switzerland) with a measurement accuracy smaller than 1 cm (Schweiger et al., 2015).

In June, July and August 2013 ground based spectral measurements and biomass samplings were carried out. An Analytical Spectral Device (ASD (ASD Inc., Boulder, CO, USA)) was used to aquire field spectroradiometer data. The ASD is a full range spectrometer and collects reflected spectra between 350 and 2500 nm in 2151 bands. The

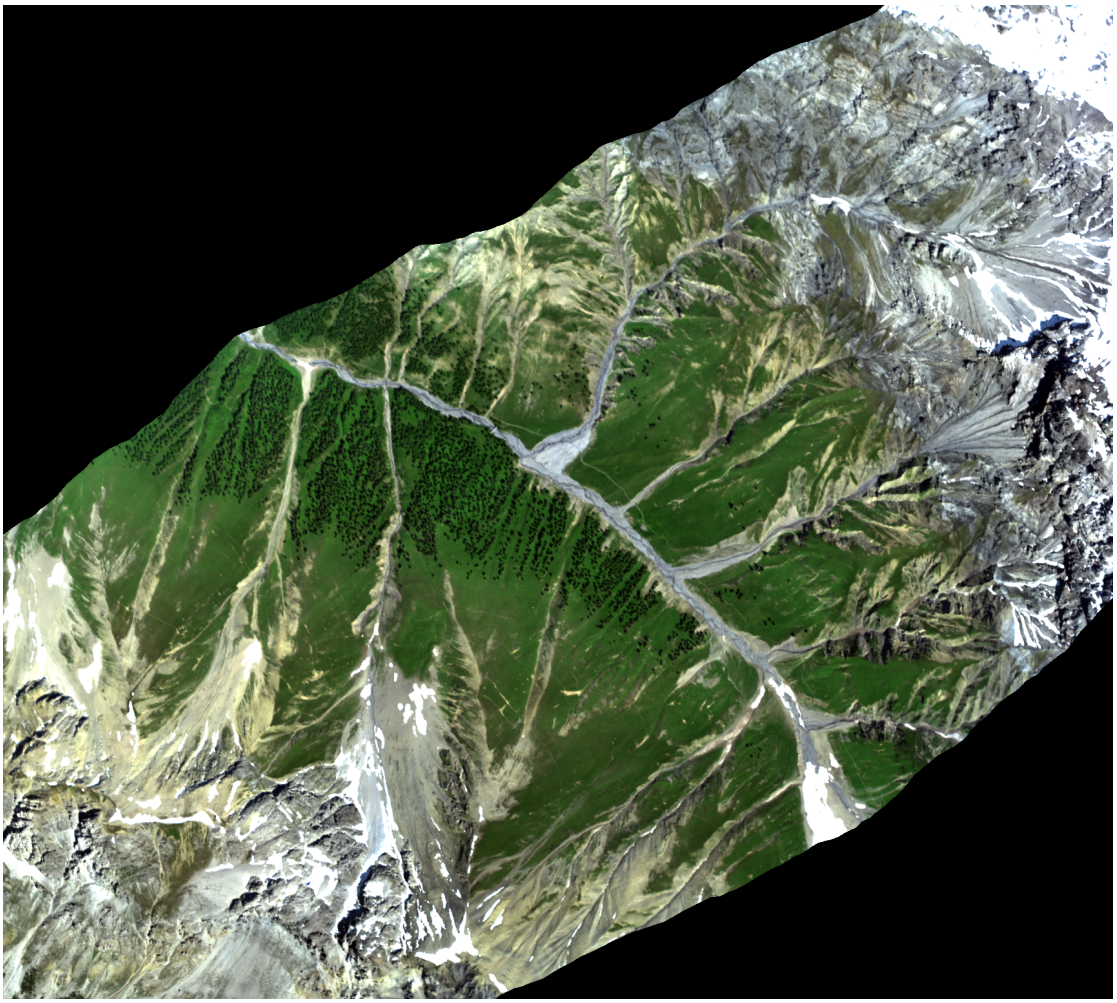

FIGURE 2.2: APEX true color image of the study area with red = 675 nm, green = 553 nm and blue = 471 nm.

spectra were collected from a height of 50 to 65 cm above ground and the sensors field of view (FOV) measured 25°. All spectral measurements were conducted under clear-sky conditions within 3.5 h before and 2 h after local solar culmination. Thirty measurements were taken of each plot. Immediately before and after, five reference measurements of a calibrated white panel, Spectralon (Labsphere Inc., North Sutton, NH, USA), were taken.

On the day of the APEX flight, 12.07.13, 20 plots were measured using the ASD device. During June and August 2013 21 plots each were sampled using the ASD. While the plots measured in June and August were the same, all but four plots measured in July were different. Table 2.1 shows a compilation of the APEX and ASD data, their date and recording time period. Within the plots, additionally 13 ASD data sets of pure vegetation and 7 ASD data sets of pure soil were taken.

		Date	Start	End	Plots	Culmination
APEX	July	12.07.13	13.52	13.58		13.26
ASD	June	16.06.13	10.13	13.07	14	13.21
		17.06.13	10.21	13.46	7	13.22
	July	12.07.13	11.38	15.08	20	13.26
	August	06.08.13	11.09	13.46	11	13.26
		12.08.13	10.20	12.43	10	13.26

Table 2.1: Recording date and time of APEX and ASD data.

The biomass samples were taken and analysed using traditional agronomic methods. To measure the total above ground biomass, the vegetation was cut 1 cm above ground along strips of 20 x 200 cm in a corner of the plot for June and August and within a 1 x 1 m square in the center of the plot for July. The fresh biomass got sealed in plastic bags and weighed on the same day to determine fresh weight. After drying the biomass for 48 hours at 65° in the laboratory, the weight of the dry biomass was determined.
Additionally, the vegetation cover ratio (VCR) of 10 plots got estimated at the peak of the growing season. 1 x 1 m squares were randomly placed within the plots and the VCR was visually estimated in percent. For all but 6 plots photos were taken showing the plots at the date of biomass cutting in June. Further plot photos from June and July 2012 are available. Table 2.2 shows the number of plots for which ASD spectra, biomass and VCR measurements and photos exist. Figure 2.3 shows the distribution of the plots within the valley, coloured according to the different kinds of measurement that were taken and the four clusters of ASD data are numbered. These cluster numbers are used in the further Chapters and Table 2.3 shows a compilation of the available field data of each cluster.

	ASD	Biomass	VCR	Photos
June	21	21		22
July	20	77	3	14
August	21	21	8	

Table 2.2: Available field data of all three months.

	ASD		Biomass		Exposition	Slope [°]	VCR [%]
	July	Jun&Aug	July	Jun&Aug			
Cluster 1		10	20	10	SW	26-40	42-63
Cluster 2		3	5	3	SW	14-19	72
Cluster 3	5	8	20	8	SW	12-33	69-84
Cluster 4	15		14		WSW	15-42	17-24 & 62-77

Table 2.3: Available field data from June, July and August, exposition, slope and vegetation cover ratio (VCR) of each plot cluster.

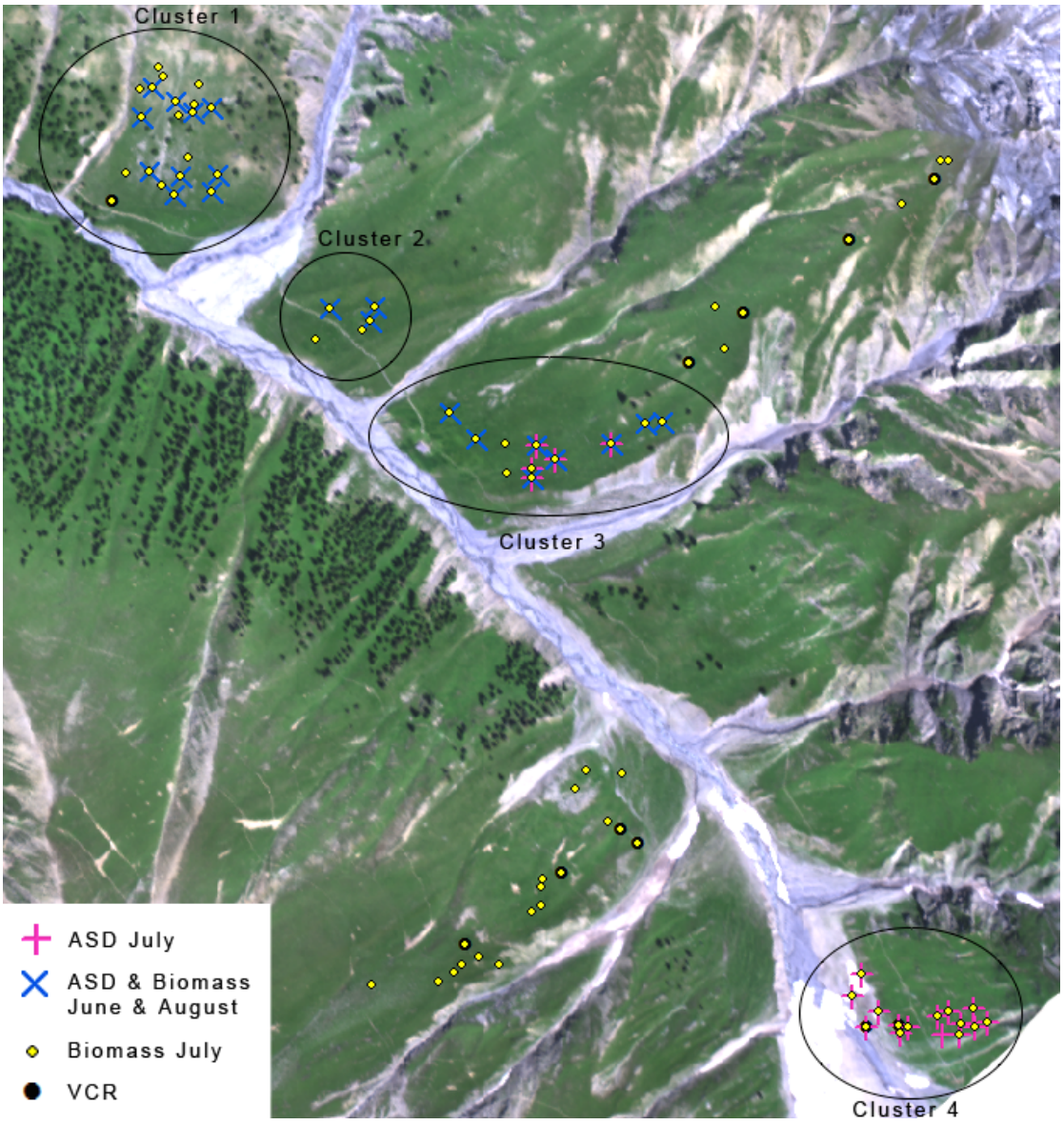

FIGURE 2.3: Plot locations, colored according to the different kind of measurements that were taken. The plots where ASD measurements were taken were grouped in four clusters. The background is an APEX true color image with red = 675 nm, green = 553 nm and blue = 471 nm.

2.3 Data preprocessing

2.3.1 ASD

The ASD data sets were stored in the spectral database SPECCHIO (Hueni et al., 2009b) and metadata was added. For each plot, the ASD reflectance factors were calculated from the 30 ASD target and the 10 ASD white reference measurements by using an interpolation over time to estimate the irradiance for each target measurement. All

reflectance spectra were convolved into APEX equivalent bands and scaled by 10^4 to correspond to the dimension of the APEX values. From the 30 reflectance spectra of each plot, the average spectrum was calculated. These preprocessing steps resulted in 20 ASD reflectance spectra for July and 21 for June and August each, that are comparable with the APEX spectra.

Reflectance factors between 1750 and 1930 nm (bands 194 to 215) had to be cut in the June and August spectra, due to culmination of outliers. In the spectra of pure vegetation and pure soil all wavelengths larger than 1750 nm (bands 194 to 284) were excluded due to unexplained spectral behaviour of single spectra and non-systematic outliers. The origin and the behaviour of the outliers will be discussed in Chapter 4.1.5.

2.3.2 APEX

The APEX pixels corresponding to the ASD plot centre coordinates and their tangent neighbour pixels were selected and stored in SPECCHIO (Hueni et al., 2009b). As these 3 by 3 pixel selections matched the 6 x 6 m plots, the mean APEX spectra for each plot were calculated.

For the creation of synthetic time series images only ASD spectra of grasslands were collected, therefore all other kinds of surface cover had to be excluded. First, a supervised classification using a maximum likelihood classifier was performed using ENVI (version 5.1, Exelsis Visual Information Solutions, Boulder, CO, USA). Regions of interest (ROI) representing rocks, snow, forest, grassland and soil were created manually. The single parts of the ROI were distributed over the whole image and each ROI included a minimum of 500 pixels.

A binary mask that excluded the areas covered by snow and rocks was generated. As forested areas and single trees could not be excluded properly by any classification method, they got identified manually and excluded from the mask as well. Adding and excluding single pixels to the mask or from the mask by a filter algorithm reduced the patchy spread. Applying the smoothed mask to the APEX data resulted in a data set containing only pixels consisting of grassland, bare soil and a mixture of both.

For the remaining data, the fraction of grass and soil for each pixel was determined. This fraction was used to further constrain the APEX data and was important for the time transformation. How the constraint was determined and why it was applied will be discussed later, as well as the importance of the fractions for the time transformation.

The chosen method was the Linear Spectral Unmixing (LSU), performed in ENVI, and the two endmembers were selected from the APEX image (Figure 2.4).

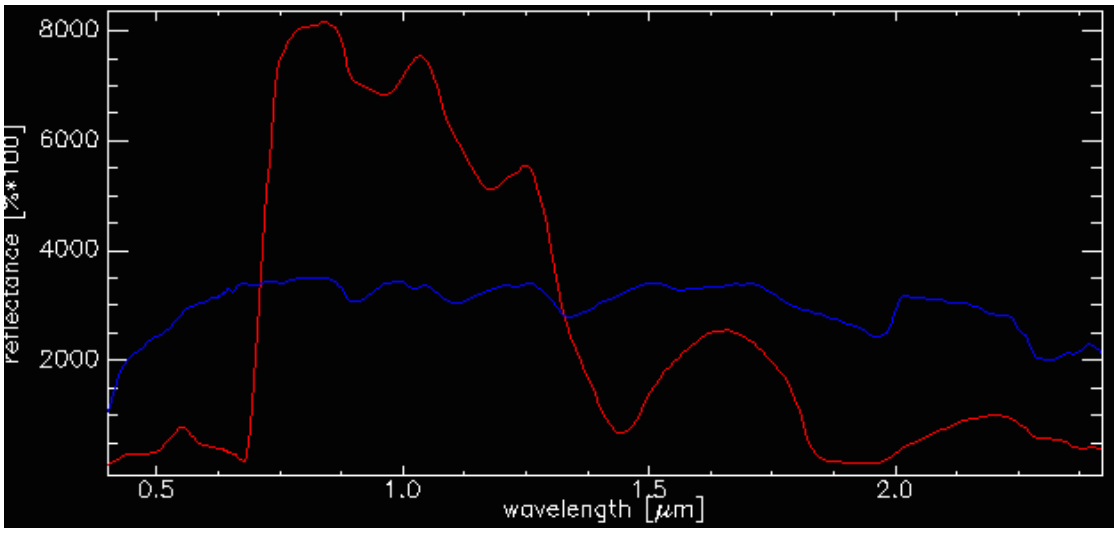

FIGURE 2.4: Endmembers of the Linear Spectral Unmixing (LSU). The vegetation endmember is displayed in red, the soil endmember in blue.

Based on the result of the LSU, each pixel obtained a VCR that stands for the percentage of vegetation cover. Additionally, the VCR was estimated in 10 plots in field at peak of growing season. Corresponding to these plot centres, 3 by 3 pixels of the VCR map were extracted for each plot and the mean VCR for each plot was calculated. For validation, these VCR values were compared to the reference VCR using linear regression.
As it was not possible to transform grasslands showing less than 40 % VCR due to the data (Table 2.3), these areas were excluded. The reasons for this exclusion are discussed in Chapter 4. Figure 2.5 shows a false colour image of the remaining APEX data.

2.4 Vicarious Validation

Before the ASD and APEX spectra were combined, I decided to do an extensive vicarious validation (VV; Small and Lu (2006)). The goal of the VV was to check if the two different kinds of data were similar enough so that they could be compared and combined. This was not the case and the data had to be adjusted. The procedure of the VV will be explained and illustrated based on the data from July.

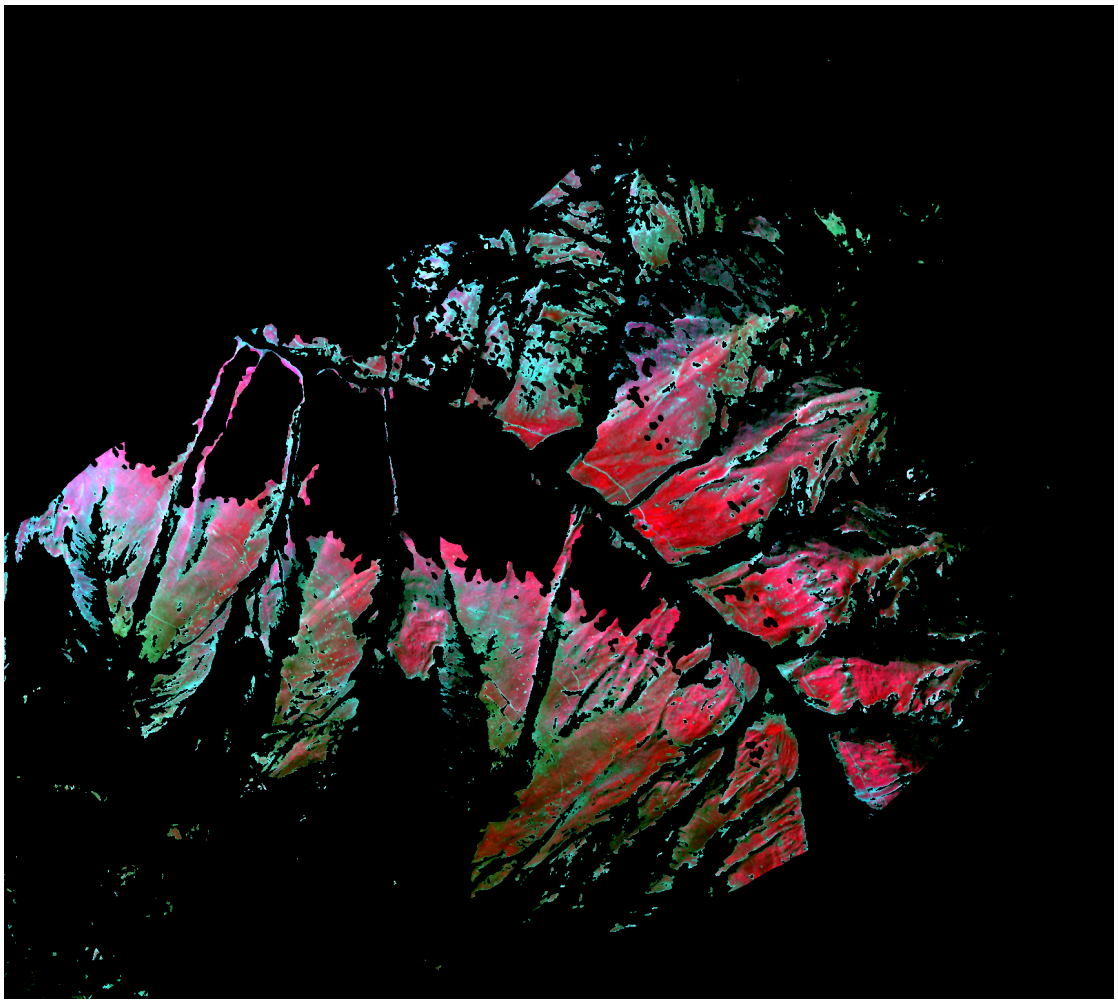

FIGURE 2.5: False colour image of the masked APEX image with red = 844 nm, green = 675 nm and blue = 553 nm. Red indicates vegetation and cyan indicates soil.

2.4.1 Spectral shift

A spectral shift was apparent in the data when visually comparing ASD and APEX spectra of the 20 plots from July. Especially in the near infra red (NIR) the local minima and maxima did not conform to each other, as can be seen in Figure 2.6a. Therefore, all the minima and maxima were distinguished and compared. Table 2.4 compiles the results.

The spectral shift was observed in the NIR and short wave infra red (SWIR) and was quite consistent over the whole data set (± 1 band), apart from some exceptions. The largest spectral shift was found at the fist maximum in the NIR and spanned across 12 bands, respectively 77 nm. The reson for the spectral shifts will be discussed in Chapter 4.1.7. The characteristics of the ASD spectra corresponded well to known absorption

	Visible		NIR			SWIR				
	max	min	max	min	max	min	max	min	max	max
ASD wvl	0.553	0.675	0.921	0.966	1.091	1.195	1.273	1.458	1.668	2.223
APEX wvl	0.553	0.675	0.844	0.900	1.035	1.166	1.254	1.449	1.659	2.202
SS [bands]	0	0	12	9	6	3	2	1	1	3
SS [µm]	0.000	0.000	0.077	0.066	0.055	0.029	0.019	0.010	0.009	0.021

TABLE 2.4: The wavelengths in micrometers of the ASD and APEX minima and maxima and the spectral shift (SS) in number of bands and micrometres.

features (e.g. Kokaly et al. (2007)). Since the goal of our work was to produce a time series of two synthetic and the original APEX image, the ASD spectra were adapted to the APEX spectra. The spectral shifts were corrected by shifting the minima and maxima and by linear interpolation of the bands in between. The same spectra as in Figure 2.6a can be seen in Figure 2.6b after the shift. The plot 89 in Figure 2.6 and three other plots of July show spectra with little resemblance to vegetation. These four plots were located in cluster 4 near the creek (Figure 2.3). The applied correction of the spectral shift is not appropriate for these plots what will be dicussed in Chapter 4.

2.4.2 Differences in the ASD data

The ASD data from July can be divided into three groups, based on their location and VCR. The three plots in Figure 2.6 represent each one plot of the three groups. Plot 65 stands for the characteristics of cluster 3, plot 96 represents cluster 4 with high VCR and plot 89 the four plots in cluster 4 with low VCR.
The plots of both clusters with high VCR are similar in VCR and the APEX spectra are comparable. However, the ASD spectra of the cluster 4 plots have much lower reflectance factors in all wavelengths. This difference cannot be explained easily and will be discussed in Chapter 4.1.

2.4.3 Transformation of the ASD spectra

The mentioned differences of the three groups of the ASD spectra from July are important for the VV, as the disparity between the ASD and APEX spectra is rather large. For all 20 plots, the ratio of the ASD and APEX spectra was calculated. This ratio is called transformation vector (TV), consists of the gain calculated for ASD and APEX spectra for each wavelength (Formula 2.4.1) and can be applied to the ASD spectra to transform

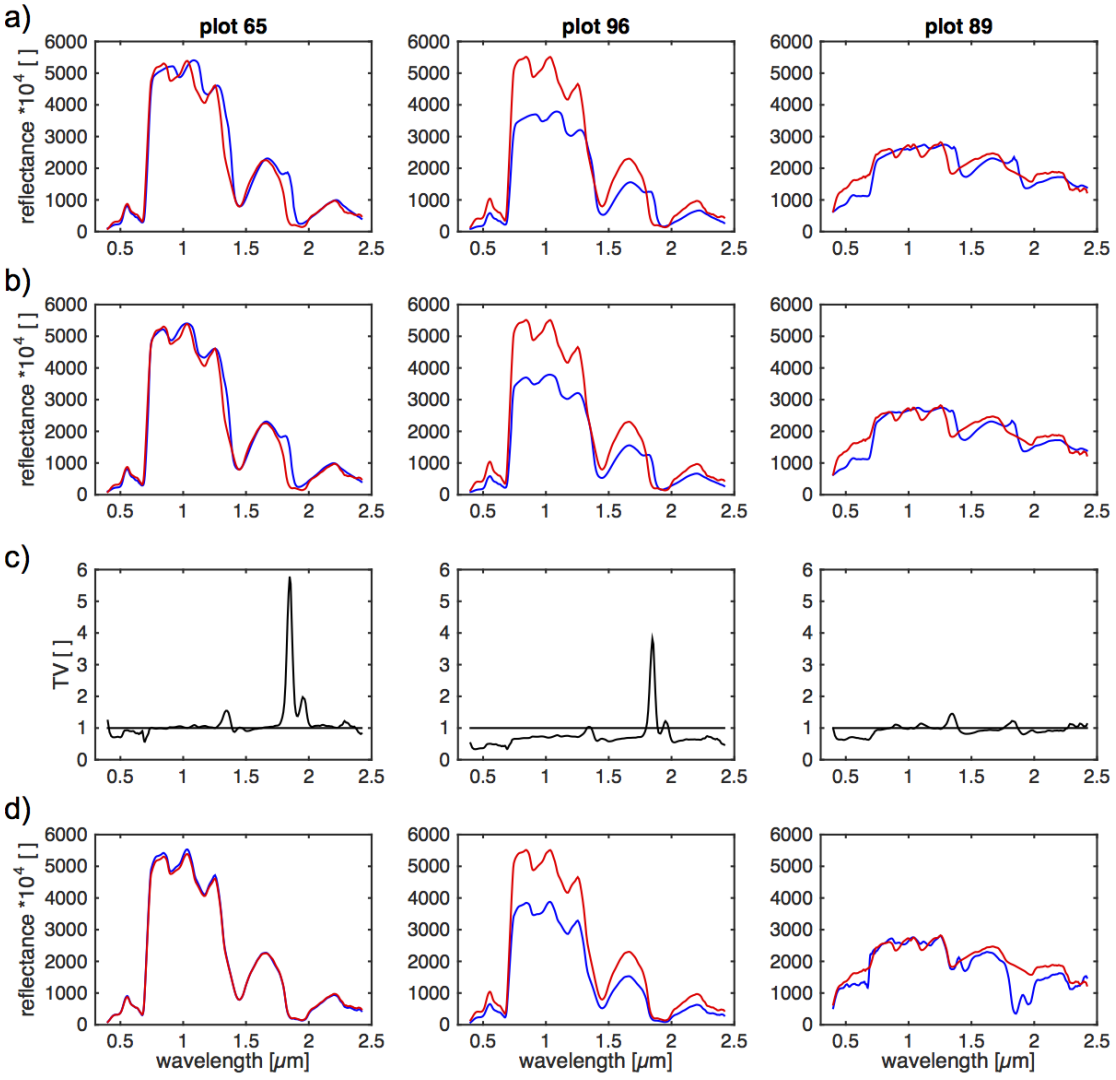

FIGURE 2.6: Three examples of the original spectra (a), the shifted spectra (b), the transformation tector (TV) (c) and the transformed spectra (d). The APEX spectra are shown in red, the ASD and the transformed ASD spectra (ASD') in blue. The plot 65 represents cluster 3 and has a vegetation cover ratio (VCR) of 71 %. The plots 96 and 89 represent cluster 4 and have a VCR of 71 % and 21 %.

it into APEX-like spectra. The transformed ASD spectra will be called ASD' (Formulae 2.4.2).

$$TV(\lambda) = APEX_{July}(\lambda) \ / \ ASD_{July}(\lambda) \tag{2.4.1}$$

$$\begin{aligned} ASD'_{July}(\lambda) &= ASD_{July}(\lambda) * TV(\lambda) \\ ASD'_{June}(\lambda) &= ASD_{June}(\lambda) * TV(\lambda) \\ ASD'_{August}(\lambda) &= ASD_{August}(\lambda) * TV(\lambda) \end{aligned} \tag{2.4.2}$$

One TV of each plot group is shown in Figure 2.5c.

The high and not completely explainable variability in the ASD data made it impossible to determine a TV that delivered reasonable results for all plots. Therefore I decided to adjust only the shape of the spectra and change the reflectance factors as little as possible.

The TVs in Figure 2.6c show that the shape of the TVs of plot 65 and 96 looked quite similar, but there is an offset. The TV of plot 65, representing the other cluster 3 plots, was around 1. Otherwise the TV of plot 96, and all other cluster 4 plots with high VCR, showed values below 1. This was due to the low ASD reflectance factors compared to the APEX reflectance factors.

To get a TV, which can also be applied to the ASD data from June and August, for which no APEX data were available for comparison, I concentrated on the cluster 3 plots, since these showed characteristic spectral behaviour and were consistent in VCR and in reflectance factors. Thus, the final TV was the ratio of mean ASD and mean APEX spectrum of the cluster 3 plots. To make sure that the reflectance factors were changed as little as possible, the sum of all reflectance factors of the original mean ASD spectrum and the transformed ASD mean spectrum were compared. Due to the high offset in the SWIR, the integral excluded the bands 197 (1798 nm) to 226 (2021nm). The TV got adjusted by 0.84% to meet the requirements of equal sum of reflectance factors before and after the transformation. Figure 2.6d shows the APEX and the transformed ASD spectra (ASD'). Again, it has to be stated that the ASD spectra of the four plots with low VCR (e.g. plot 89) could not be adjusted appropriately. These plots and, as already mentioned, all APEX pixels having less than 40% VCR were excluded from further analyses. The TV was applied to the ASD spectra of June and August (ASD', (Formulae 2.4.2)).

2.5 Time Transformation

The core element of this master thesis was to create two a synthetic time series of APEX images from June to August. Together with the original APEX data from July, they resulted in a synthetic APEX time series, consisting of these three data sets.
To transform the APEX data from July to June and August respectively, a time transformation tunction (TTF) was determined. The TTF was based on the difference of the 21 ASD' spectra from June and August respectively and the corresponding APEX spectra from July. An appropriate overall TTF had to be found, for time transformations from July to June and July to August respectively, and it had to be applied to the APEX data from July. The synthetic APEX data was validated using ground based biomass samplings.
The determination and application of the TTF is explained and illustrated based on the time transformation July-August below.

2.5.1 Time Transformation Function

The TTF was based on the difference of the ASD' spectra from August (respectively June) and the APEX spectra from July for each plot (Formulae 2.5.1). The transformation of the ASD spectra to APEX-like spectra (ASD') rendered them comparable. The single TTFs for each plot were calculated and are displayed in Figure 2.7. The TTFs are coloured according to their VCR. Generally it can be seen that for nearly all plots and in almost all bands, reflectance factors in August were lower than in July (TTF were lower than 1).

$$\begin{aligned} TTF_{June}(\lambda) &= ASD'_{June}(\lambda) \ / \ APEX_{July}(\lambda) \\ TTF_{August}(\lambda) &= ASD'_{August}(\lambda) \ / \ APEX_{July}(\lambda) \end{aligned} \tag{2.5.1}$$

In the beginning of this master thesis there consisted the assumption that the change in time depends on the vegetation cover. There was a dependency on VCR as different data analyses showed, but it was inconsistent, as is discussed later in Chapter 4.1.7. As there was no meaningful way to create TTF dependent on VCR, I chose the mean of all TTF as TTF for the transformation of the APEX data. The TTF was applied to the

original APEX image (Formulae 2.5.2) and resulted in the synthetic APEX image for June (APEX'June) and August (APEX'August).

$$\begin{aligned} APEX'_{June}(\lambda) &= TTF_{June}(\lambda) * APEX_{July}(\lambda) \\ APEX'_{August}(\lambda) &= TTF_{August}(\lambda) * APEX_{July}(\lambda) \end{aligned} \tag{2.5.2}$$

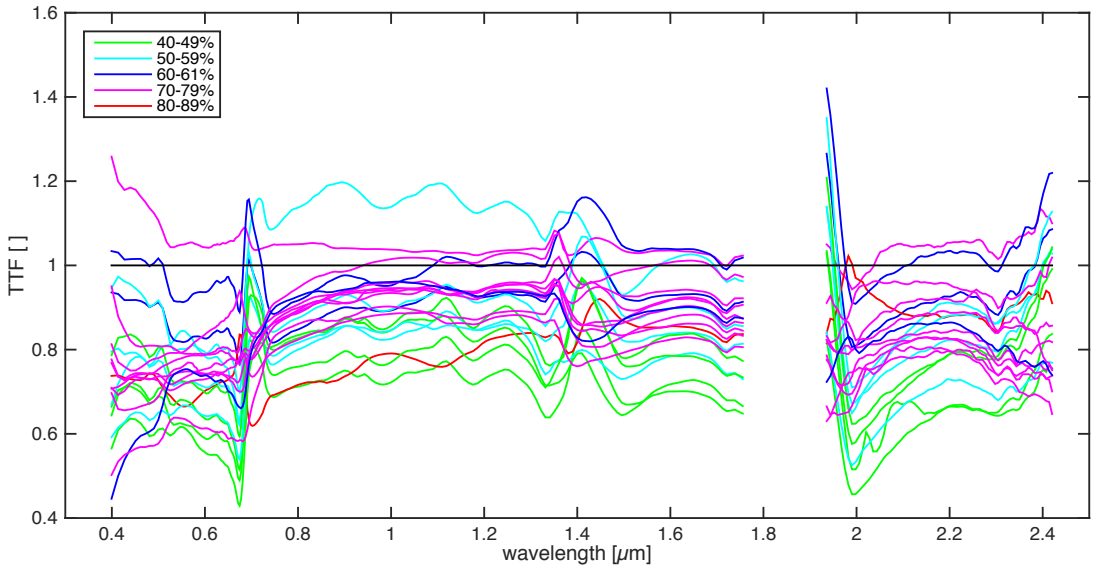

FIGURE 2.7: All time transformation functions (TTF) from August, coloured according to the vegetation cover ratio (VCR) of their plot.

2.5.2 Validation

For validation, a model linking the Normalized Difference Vegetation Index (NDVI; Rouse et al. (1974); Tucker (1979)) to wet biomass field measurements was established. To calculate the NDVI for the APEX and ASD' data, the red minimum at 675 nm and the first maximum in NIR at 844 nm were used, while for the the original ASD data, the fist maximum in NIR at 921nm was used.

For the ASD and ASD' data, each from June, July and August, six exponential models predicting biomass based on NDVI were built and validated using leave one out cross validation (LOO-CV; Cawley and Talbot (2004)). For June and August, biomass data from 21 plots were used, while for July, one plot had to be excluded because of a missing biomass value, resulting in 19 plots for modelling.

To model the biomass based on NDVI for the original APEX data, a cross validation (CV; Diaconis and Efron (1983)) was conducted. For July, there were biomass measurements of 77 plots. Corresponding to these plots, again 3 by 3 APEX pixels aggregation was used to extract the reflectance factors and calculate the mean spectra and NDVI, respectively. The plots were sorted according to their NDVI values and every 4th plot was used for model validation, resulting in 51 training and 19 validation plots.

As only 21 biomass measurements from August were available, a LOO-CV was performed for validation of APEX'August.

All regression analysis performed in this thesis were based on a level of significance of 0.05 and were calculated with MATLAB (version R2014b, The MathWorks, Natick, MA, USA).

Chapter 3

Results

In this Chapter I present first the results from the data preprocessing, namely the results of the classification and the spectral unmixing and the validation of the unmixing. Second, the results of the biomass models based on ASD, ASD', APEX and APEX' data are shown.

3.1 Data preprocessing

3.1.1 Classification

The prerequisite of the classification was to exclude areas that comprise no vegetation, on the condition that all plot locations remained in the data. Different algorithms provided by ENVI were tested and the maximum likelihood classifier performed best (Figure 3.1). Areas covered by rocks and snow were distinguished easily by this classifier. These two classes matched well when visually compared to the true colour or false colour image. All plot locations remained in the classes vegetation and soil. It was not possible to exclude the patchy forest and single trees using an algorithm. Therefore forests and single trees had to be excluded manually.

In the classified image an artefact originating from the APEX raw data became apparent. Two wires are placed in the entry slit of APEX to observe spatial shifts. Depending on the geometric shifts, some remaining wire residuals may exist. These linear artefacts are

a matter of the linear interpolation during level 1 processing. The interpolated region currently encompasses a buffer of 1 pixel around the wire positions (across track, pixels 334-335 and 674-675). Pixels in the interpolated wire region should be treated with caution. In this case, they were neither visible in the true colour nor in the false colour image, but appeared in the classified image as double lines in the northern part of the image and as single line in the southern part (Figure 3.1).

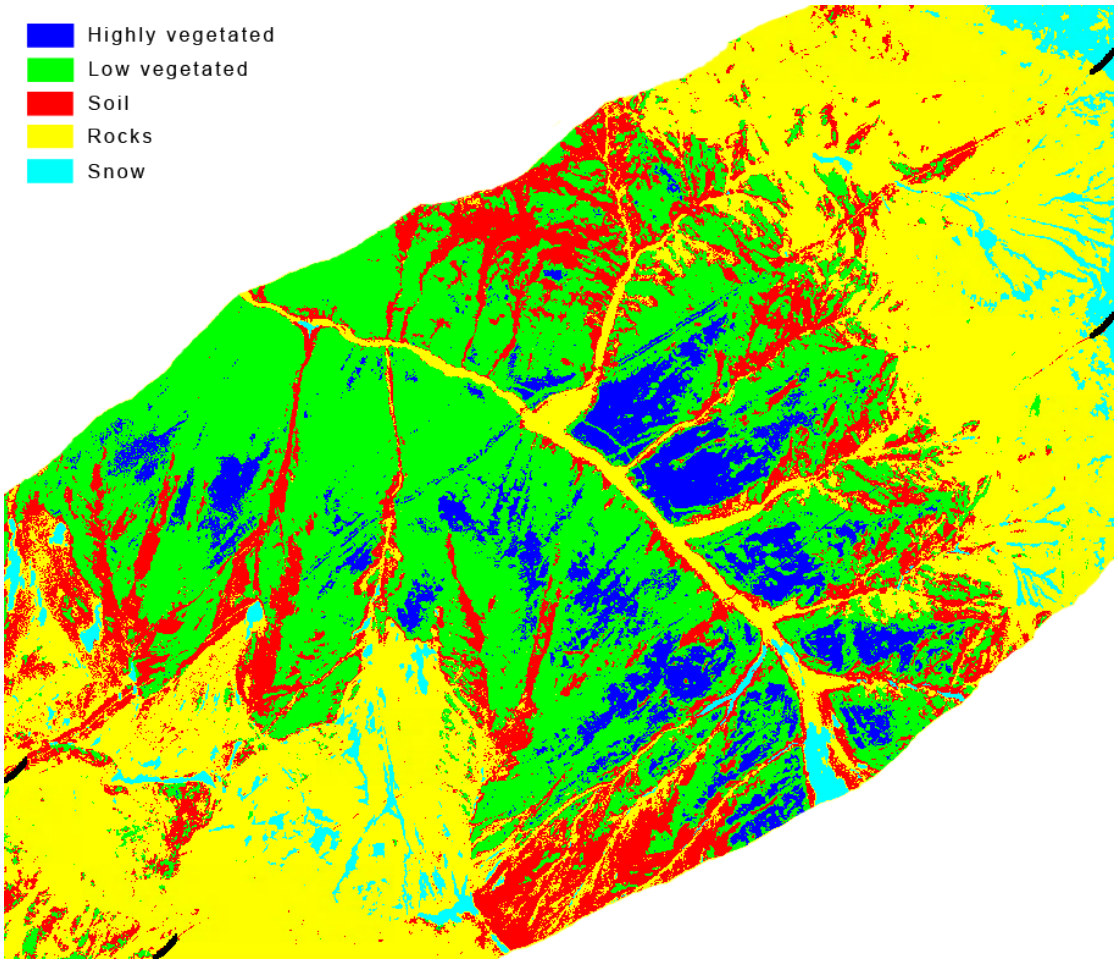

FIGURE 3.1: Result of the APEX classification. The two wire artefacts are visible as double line (upper wire) and as single line (lower wire). The four black lines at the edges of the images indicate the position of the two wires.

3.1.2 Unmixing

Linear Spectral Unmixing (LSU) of grassland and soil resulted in the vegetation cover ratio (VCR), that is the amount of vegetation cover per pixel. The VCR was measured in 10 plots in field at peak of growing season. The regression showed a strong positive correlation ($R^2 = 0.94$) between the estimated and measured data. The ANOVA was

significant but the constant of the regression function was not significant as there was a leverage effect. This was caused by the inordinate distribution of the plots concerning their VCR. Figure 3.2 shows that the VCR was underestimated. Possible reasons are discussed later on in Chapter 4.2.

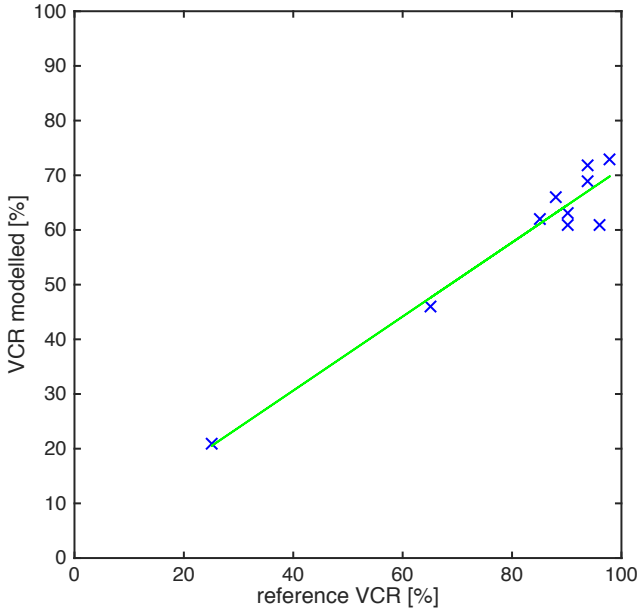

FIGURE 3.2: The linear regression of the vegetation cover ratio (VCR) had an R^2 of 0.94 but showed a leverage effect due to the inordinate distribution of the plots concerning their VCR.

3.2 Biomass models

As already explained in Chapter 2.5.2, an exponential regression model linking the Normalized Difference Vegetation Index (NDVI; Rouse et al. (1974); Tucker (1979)) and wet biomass was established. It was used to validate the transformation from ASD to ASD' data and for the validation of the APEX data transformed to June and August (APEX').

3.2.1 ASD and ASD'

For the ASD and ASD' data, from June, July and August, six exponential models predicting biomass were built and validated using leave one out cross validation (LOO-CV; Cawley and Talbot (2004)). The transformation from ASD to ASD' was designed to adjust the shape of the spectra, changing the values only minimally, with the sum of all

reflectance factors staying the same. Therefore, no difference in the performance of the models based on ASD and ASD' data was expected. Figures 3.3, 3.4 and 3.5 show the models and the regression analysis for June, July and August.

The differences between the ASD and ASD' data is minimal for all months. There is hardly any visual difference and the R^2 values remained the same for June and August and were marginally different for July.

Another important aspect was to test the performance of the model using ASD reflectance factors to predict biomass values. The results turned out very different. The models from August showed a significant, positive correlation ($R^2 = 0.60$) between estimated and measured biomass. In contrast to August, the model from June performed very weakly, even though the ASD data from June and August comprised samples from the same 21 plots. The correlation in June was statistically not significant ($R^2 = 0.16$). The correlation for the July data was moderatly positive and significant with an R^2 of 0.38 for ASD data and 0.37 for ASD' data.

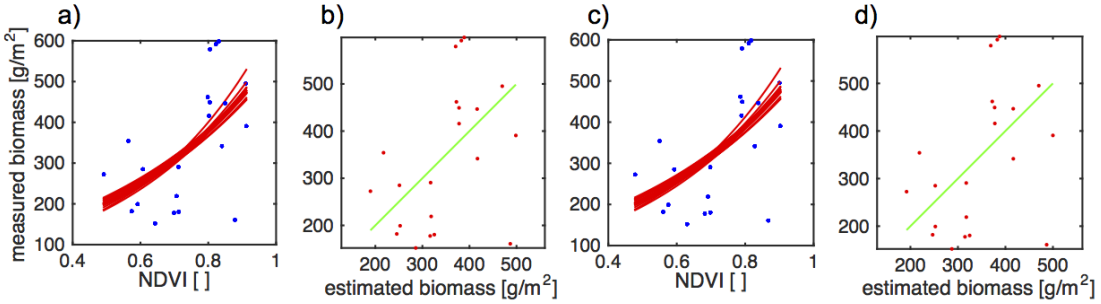

FIGURE 3.3: The Figures a) and c) show the biomass models of ASD (a) and ASD' (c) from June. For both models the correlation of measured and estimated biomass showed an R^2 of 0.16 (b and d).

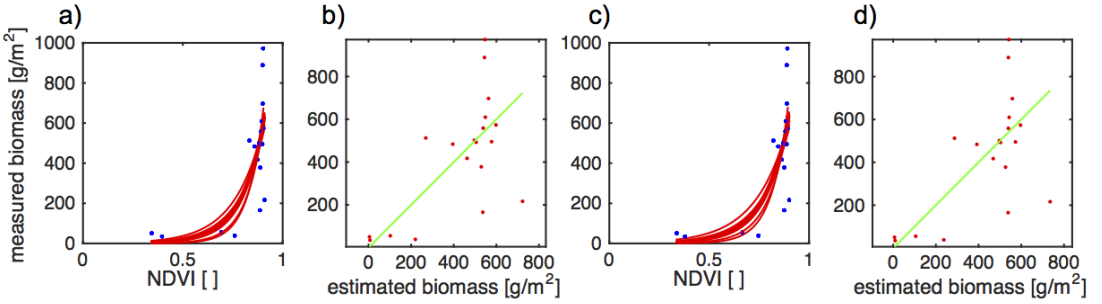

FIGURE 3.4: The Figures a) and c) show the biomass models of ASD (a) and ASD' (c) from July. For the ASD model the correlation of measured and estimated biomass showed an R^2 of 0.38 (b) and for the ASD' model an R^2 of 0.37 (d).

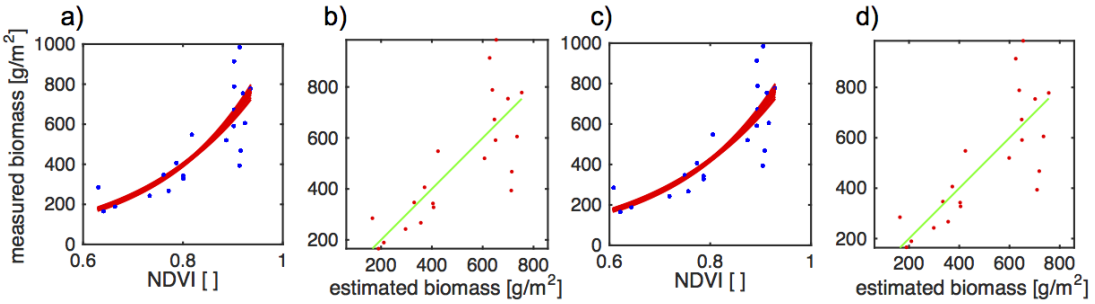

FIGURE 3.5: The Figures a) and c) show the biomass models of ASD (a) and ASD' (c) from August. For both models the correlation of measured and estimated biomass showed an R^2 of 0.60 (b and d).

3.2.2 APEX July

Before the biomass model could be used for validation of the synthetic APEX data, the performance of the model had to be tested based on the original APEX data. Therefore, a cross validation (CV; Diaconis and Efron (1983)) was performed using the 77 biomass measurements from July and the corresponding 3 by 3 APEX pixels from July (Chapter 2.5.2). The R^2 calculated for the 19 reference plots measured 0.27 and the correlation was moderatly positive and significant. The model and the result are displayed in Figure 3.6.

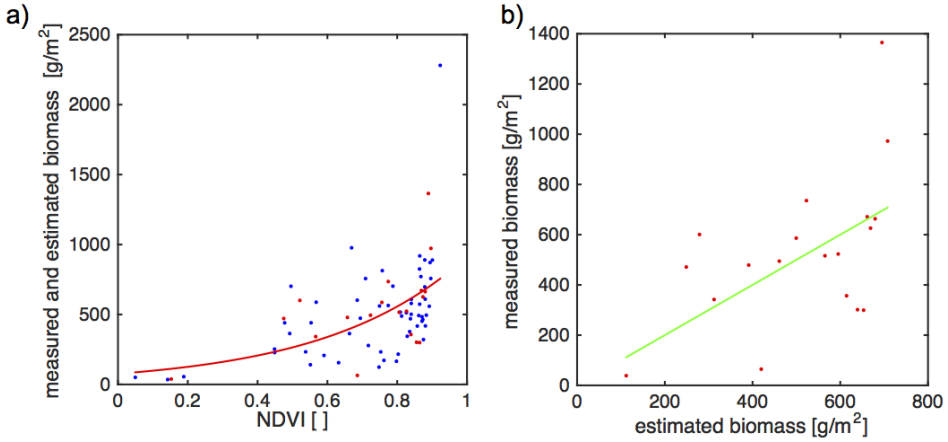

FIGURE 3.6: These Figures show the biomass model (a) based on the APEX data from July and its validation (b). In Figure a) the measured values are in blue and estimated values in red. Figure b) shows the correlation of measured and estimated biomass with an R^2 of 0.27.

To compare the performance of the model based on ASD data with the model based on APEX data, two additional LOO-CV were carried out. Consequently only the biomass

and the 3 by 3 APEX pixels that conformed to the 19 plots of the July ASD measurements out of the 77 plots were used. The same was conducted for the 21 plots corresponding to the June and August ASD measurements. The observed differences between ASD and APEX data were converse. For July, the APEX model showed a significant and strong positive correlation (R^2 = 0.82). This performance was better than basing the model on the ASD data (R^2 = 0.38). However, the model designed based on data of the plots from ASD June and August showed no correlation. The negative R^2 of -0.10 is evidence that the chosen exponential model fit the data poorly and was not the appropriate one for this data. Both models and correlations can be seen in Figure 3.7.

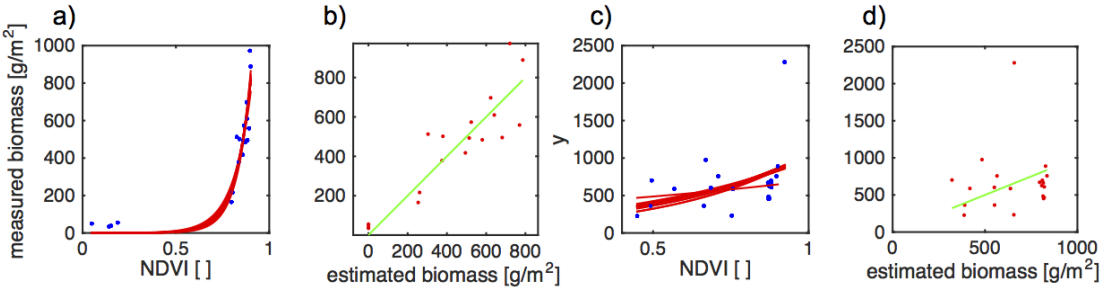

FIGURE 3.7: The Figures a) and b) show the biomass model and its validation based on APEX spectra corresponding to the 19 July plots. The correlation of measured and estimated biomass (b) showed an R^2 of 0.82.
The Figures c) and d) show the biomass model and its validation based on APEX spectra corresponding to the 21 June and August plots. The correlation of measured and estimated biomass (b) showed an R^2 of -0.10.

3.2.3 APEX' June and August

Model validation (LOO-CV) for the APEX'August showed a significant, moderate correlation (R^2 = 0.56, Figure 3.8). The model performed better than the one based on the 77 APEX plots from July (R^2 = 0.27, Figure 3.6) and the one based on the same 21 APEX plots from July (R^2 = -0.10, Figure 3.7, the two right plots), providing evidence that the chosen exponential fit was appropriate for the APEX'August data.

Model validation for the synthetic APEX data from June (APEX'June) resulted in a significant and moderatly positive correlation (R^2 of 0.35, Figure 3.9). Again, this model is slightly better than the one based on the 77 plots from July (R^2 = 0.27, Figure 3.6).

Table 3.1 summarises the validation results of all biomass models that have been performed.

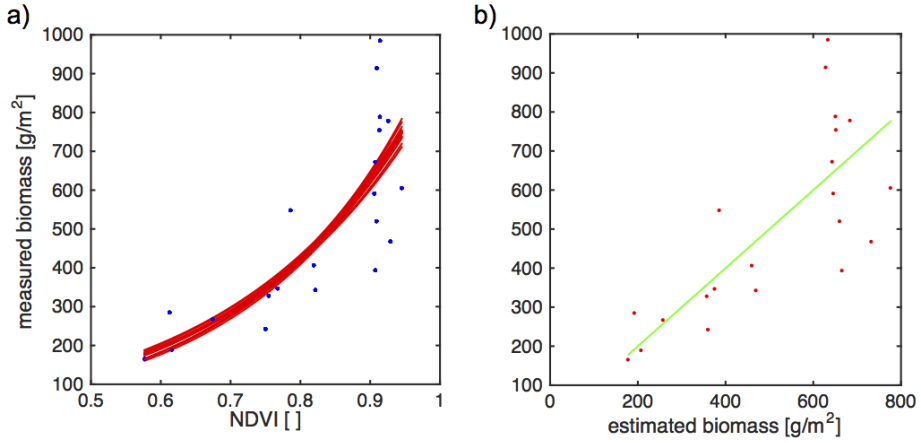

FIGURE 3.8: These Figures show the biomass model (a) based on the APEX'August and its validation (b). The correlation of measured and estimated biomass (b) had an R^2 of 0.56.

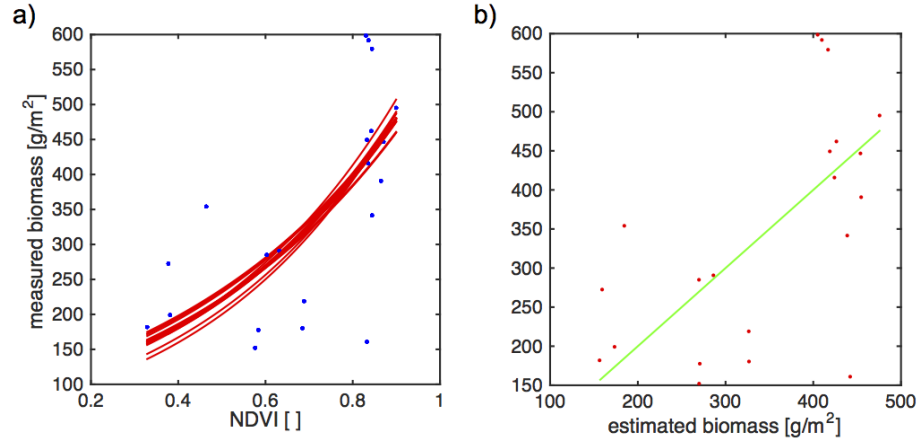

FIGURE 3.9: These Figures show the biomass model (a) based on the APEX'June and its validation (b). The correlation of measured and estimated biomass (b) had an R^2 of 0.35.

	ASD			APEX	APEX'	
	June	July	August	July	June	August
21 plots June & August	0.16		0.60	-0.10	0.35	0.56
19 plots July		0.37		0.82		
77 plots July				0.27		

TABLE 3.1: Summary of the R^2 of all biomass models. The first row is related to models based on the 21 plots of the ASD measurements from June and August, the second row on the 19 plots from July and the third row on the 77 plots of the biomass measurements from July.

Chapter 4

Discussion

In this Chapter I discuss the data used in this study and its suitability concerning the combination of airborne and ground based spectral data. Further, I analyse the different steps of the working process, discuss the results and answer the hypothesis proposed in Chapter 1.4.

4.1 Data

In contrast to other studies where airborne or satellite based data were combined with ground based spectral measurements (e.g. Boschetti et al. (2007), Numata et al. (2008)), I performed a detailed vicarious validation (VV; Small and Lu (2006)). First, the ASD and APEX data were examined separately and then compared. This Chapter looks for explanations for the characteristics and behaviour of the data.

As mentioned in Chapter 2, there were differences in the ASD data that could not be explained easily and due to the varying characteristics of the data, some ASD spectra had to be excluded from the creation of the transformation vector (TV) and the time transformation function (TTF). The following paragraphs give more details about the ASD spectra and discuss the differences between ASD and APEX data.

4.1.1 Plot distribution

The ASD plots were grouped into four clusters to enable ASD measurements and biomass harvesting within a short time. Especially at the day of the APEX over flight it is important to take the ASD measurements within a short time frame before and after the over flight (Schweiger et al., 2014) due to the changing illumination geometry. The four plot clusters were on the same side of Val Trupchun all facing southwest to west-southwest (Figure 2.3). The slope of the ASD plots ranged from 12 to 42 degree.
However, there were systematic differences in the ASD measurements from July. The cluster 4 plots (Figure 2.6 middle) and the cluster 3 plots (Figure 2.6 left) were similar in vegetation cover but the range of the ASD reflectance factors differed much. The spectra of cluster 4 show lower values compared to the ones of cluster 3 and compared to the corresponding APEX spectra, whereas for the cluster 3 plots the ASD and APEX spectra match well. The exposition of the two clusters does not differ much but the slope of cluster 4 is steeper. As the ASD pistol was held vertically to the slope and APEX's fied of view is almost perpendicular, the steeper the slope the higher is the viewing angle difference between ASD and APEX. Steep viewing angles, as with APEX, give a more direct view to the ground than flat viewing angles. This could result in spectra showing less vegetation characteristics, but this is not the case here as the ASD and APEX spectra show the same characteristic, with differences evident only among reflectance factors. In the APEX data, the influence of exposition and slope was corrected during irradiance correction in ATCOR (Schweiger et al., 2014). This can be confirmed, as the APEX data of the plots show no variation regarding exposition or slope.

4.1.2 Recording time and illumination geometry

Additionally, the recording time of the ASD spectra, and consequently the illumination geometry, could have influenced the reflectance factors. The reflectance factors were normalised, based on the radiance measurements of the target and the white reference (WR). The acquisition time of the ASD spectra should be shortly before or after the APEX over flight. In this case, the cluster 4 plots were measured up to two hours before the APEX over flight and before and during solar culmination, while the cluster 3 ASD spectra were recorded up to one hour after the APEX over flight. In June and August all ASD measurements but two were taken before solar culmination and all ASD

measurements were taken before the time of the APEX over flight from July.

To evaluate if the recording time could have an influence on the ASD measurements, all WR spectra were compared. Highest WR radiance values were expected for June (closest to solstice on 21.06.) and around solar culmination from 13.21 to 13.26 o'clock CEST. Figure 4.1 shows the radiance values of all WR spectra at a wavelength of 500 nm (ASD band 151), corresponding to the solar irradiance maximum. As expected, a slight increase before and a slight decrease after solar culmination can be seen in the WR radiance values but no evident differences between the three months can be distinguished. More noticeable was the scattering of the radiance values between 0.1 and 0.6 W/sr/m^2. Even within one plot the values differed up to 0.4 W/sr/m^2 implying an increase of 400 % from the first WR measurement to the last, occuring within three minutes (plot 91, 12.7.13, 15.06-15.09 o'clock). As the dimension of these variations were not explained by normal irradiance changes on a cloud free day within some minutes (pers. communication by A. Hueni), they were based either on instrumental error or on an inaccurate measurement process.

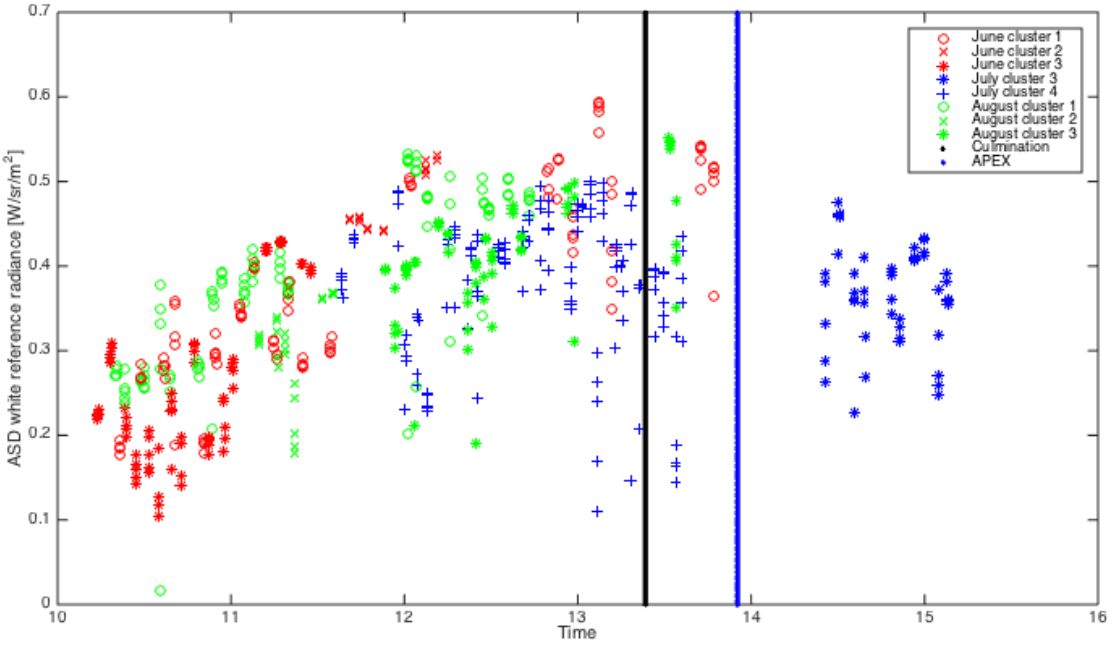

FIGURE 4.1: Radiance values of all white reference (WR) spectra at a wavelength of 500 nm, measured at different times. The measuremets taken in June are in red, the measurements from July in blue and from August in green. The symbols indicate the cluster the measurements were taken at. The black and the blue line indicate the time of culmination and of the APEX over flight.

4.1.3 Sampling design

For the sampling design some points can be criticised. The first main issue is related to the handling of the WR and the ASD pistol. As already mentioned, the ASD pistol was held vertically to the slope, contrary to the APEX's view that was almost perpendicular. In a flat area, the ASD measured direct and indirect reflections from the vegetation and the soil. The steeper the slope the less direct reflections the ASD measured from ground. However there seemed to be enough indirect reflection coming from ground that was measured by the ASD, as the reflectance characteristic of steeper plots was not dominated more strongly by vegetation characteristic than less steep plots with the same VCR.

The WR was held vertically to the slope as the ASD pistol. This procedure is controversial, hence it is analysed in the following paragraphs.

When ASD measurements are taken in flat terrain, the WR is sited on the ground i.e. perpendicular to the gravitational vector. In ATCOR the irradiance on the ground and thereby the reflectance factors are calculated for the APEX image. Therefore, the two data types are comparable as the sensor and illumination geometries match.

In a rugged terrain, as in this study area, ATCOR applies a topographic correction based on a digital elevation model (DEM) to the APEX data, i.e. the irradiance that reaches a pixel is calculated for every pixel. For an ideal reflectance factor data cube, the reflectance factors correspond to the property of the surface and the data is not affected by shadows or hill shading.

For the ASD, the irradiance is approximated by WR radiance measurements. The WR has to be held parallel to the slope and the ASD pistol vertical to the WR to receive as much energy as the target on the slope that is to be measured. This approach was chosen for this study and lead to high scattering in the WR radiances (Chapter 4.1.2). A suggestion for improvement is to place the WR on a tripod and exposing it in the same way as the slope than laying the WR on the ground or holding it manually.

An alternative approach can be to measure with a perpendicular WR in the field and then correct the panel irradiance using the same DEM that is used to correct the APEX data set.

A third approach for the ASD reflectance factor calculation can be to simulate the solar irradiance for each plot corresponding to its exposition, slope and point in time of the ASD target measurements in ATCOR as it is done for APEX. However, this would have

required reliable parameters for the ATCOR correction that were not given in this case (Chapter 4.1.7).

The handling of the WR is not the only crucial point for an appropriate ASD reflectance factor. The different dates, times of the day and varying expositions and slopes can also affect the measurements.

The second main criticism on the sampling design regards the inequality and incompleteness of the measured data. The measurements have not been taken consistently: the ASD measurements of the three months were not based on the same plots, there was not the same number of biomass measurements for the three months and photos of the plots were only taken randomly. This fragmentary data basis complicated the examination of the data during the vicarious validation (VV) process or made it even impossible. The next Chapter presents an example showcasing this problem.

4.1.4 ASD data from June and August

Some inconsistencies were observed when comparing the ASD measurements from June and August within the same month and to the measurements from July. In contrast to the July measurements, in June there were no distinct differences in the spectra among the three plot clusters or the two measurement days. It was apparent that the range of the ASD reflectance factors was higher than the APEX reflectance factors. Additionally, there was one outlier in the ASD data with reflectance factors nearly up to 90 % (plot 64), which is far above the regular range of values. Figure 4.2a shows the ASD spectra and Figure 4.2b depicts the APEX spectra from June coloured by their vegetation cover ratio (VCR). Higher VCR were expected to lead to higher reflectance factors in the near infra red (NIR). While this was indeed observed in the APEX spectra, the characteristic of the ASD spectra from June differed.

The outlier from June (plot 64) was one of the steepest plots and could therefore, as already discussed, have had high reflectance factors observed based on its steepness. On the other hand, the ASD measurements of this plot taken in July and August were within the normal range. In this case, as three spectra of the same plot could be compared, it was possible to make a statement about the reliability of an ASD measurement. In this case the ASD measurement from June of plot 64 was inaccurate. However, as only four plots were measured in all three months (June, July and August) there mostly

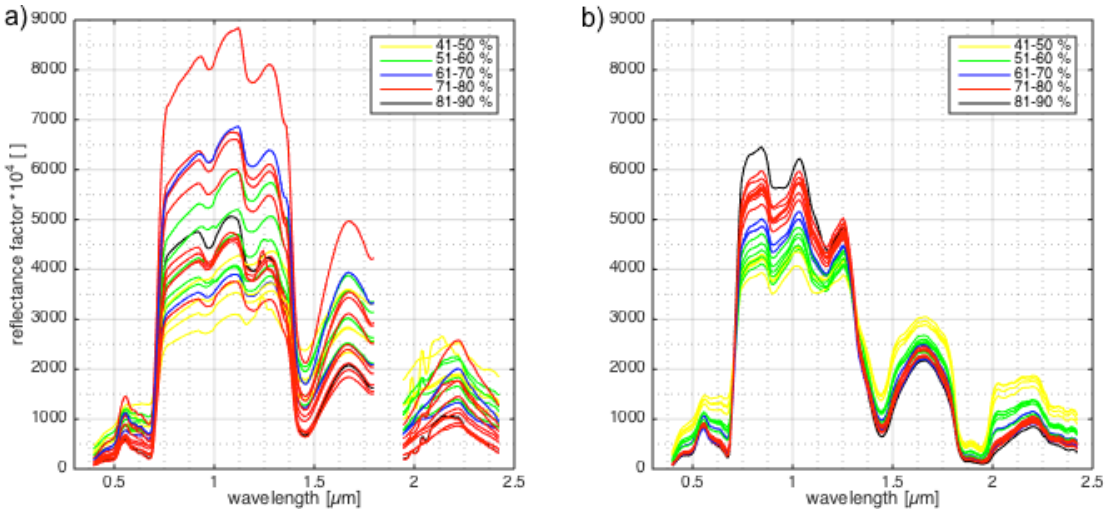

FIGURE 4.2: ASD spectra from June (a) and corresponding APEX spectra from July (b), both coloured by their vegetation cover ratio (VCR).

was no data allowing judgements about the accuracy of the data or finding reasons for deviations. This was one of the major difficulties of this thesis and was caused by the fragmentary data basis.

The ASD data from August showed differences between the three plot clusters. These differences in August, that were also slightly visible in the spectra from June, could be traced back to different VCR. Based on the ASD spectra of the three months it could be stated that the VCR had a more evident influence on the ASD spectra with more successive phenological state of the vegetation (Figure 4.3).

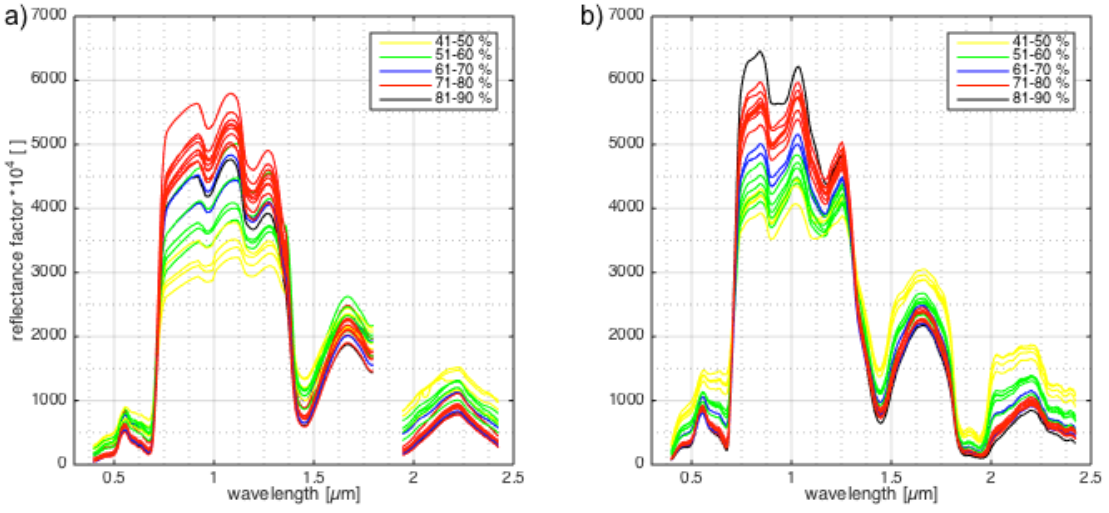

FIGURE 4.3: ASD spectra from August (a) and corresponding APEX spectra from July (b), both coloured by their vegetation cover ratio (VCR).

4.1.5 Outliers in the ASD spectra

As mentioned in Chapter 2.3.1, some parts of the ASD spectra had to be excluded. Figure 4.4 shows the 30 ASD reflectance spectra of plot 1 from June. There were several wavelengths showing outliers and some of them corresponded to the interpolated APEX bands (Table 4.1). When the mean of the 30 spectra was calculated most of the outliers were eliminated, only the spectra between 1800 and 2000 nm remained affected by outliers. These outliers originate from the division of divisors (WR radiance) and dividends (target radiance) both with values near zero caused by strong water vapour absorption of these wavelengths in the atmosphere.

The alternative to cutting these wavelengths is an interpolation as it is done for the APEX data. Due to the problem of the spectral shift between ASD and APEX and due to the fact that the interpolated bands in APEX show probably wrong values (Chapter 4.1.7) no interpolation was performed.

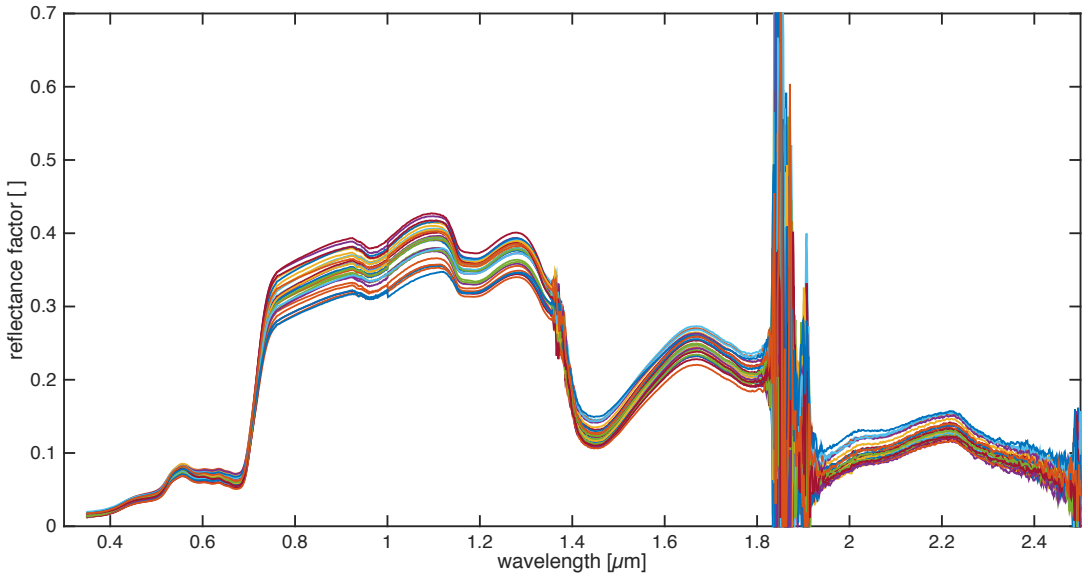

FIGURE 4.4: The 30 ASD reflectance factor spectra of plot 1 from June show the wavelengths affected by outliers.

4.1.6 Spatial shift

Corresponding to the ASD data, the APEX reflectance spectra were extracted and compared. Possible geometric mis-registration of less than 2 m in flat terrain and up to 4 m on steep slopes (Damm et al., 2012) raised the question how to determine the APEX

spectra for the plots where the ASD spectra were measured. As the plots were located in homogeneous areas, a spatial shift of 1 to 2 pixels is expected not to have a high impact on the data. However, additionally to the 3 by 3 pixels extraction, which corresponds to the 6 x 6 m plot size, only the centre pixel and an area of 5 by 5 pixels were extracted. This was performed based on the APEX image and on the VCR image. The mean spectra of the 9 pixels, the 25 pixels and the spectra of the centre pixel showed nearly no difference when visually compared, just as the mean VCR values differed in 0-1 % only. These findings do confirm that the plots were indeed placed in homogeneous areas and that errors due to inaccurate geocorrection and co-registration had most likely a diminishing impact.

4.1.7 Atmospheric compensation problems

The spectral shift that appeared when the ASD and APEX plot reflectance spectra were compared can be attributed to the APEX data. This is evident if the extrema of the spectra are compared with those found in the literature (e.g. Kokaly et al. (2007)) and within APEX data of different locations (e.g. Oensingen, 01.07.13). While it may look like a spectral shift, the actual reason is a wrong atmospheric correction that leads to spectral features where there should be none. This is apparently linked to wrong water vapour estimation in ATCOR, leading to wrong irradiance values and probably to wrong interpolation results (pers. communication by D. Schlaepfer). For this reason, the interpolated APEX bands shown in Table 4.1 should be used carefully.

Range	Bands	Wavelength [μm]
Red edge	56 - 68	0.691 - 0.736
NIR	72 - 76	0.753 - 0.771
NIR	81 - 89	0.795 - 0.838
NIR, water absorption	99 - 111	0.900 - 0.992
NIR, water absorption	123 - 132	1.100 - 1.185
water absorption	147 - 163	1.331 - 1.486
SWIR, water absorption	196 - 221	1.781 - 1.983

TABLE 4.1: Interpolated APEX bands.

As the distinguished minima and maxima of the ASD and APEX spectra were quite consistent (mostly $\pm$ 1 band), a general transformation function to shift the ASD data was applied. This approach still led to persisting spectral shifts in some ASD spectra of June and August around the second maximum in NIR at 1.035 μm (Figure 4.5).

This shift was only related to ASD data obtained on certain dates and not all spectra of these dates were affected. These artefacts cannot be explained and depict another inconsistency in the ASD measurements.

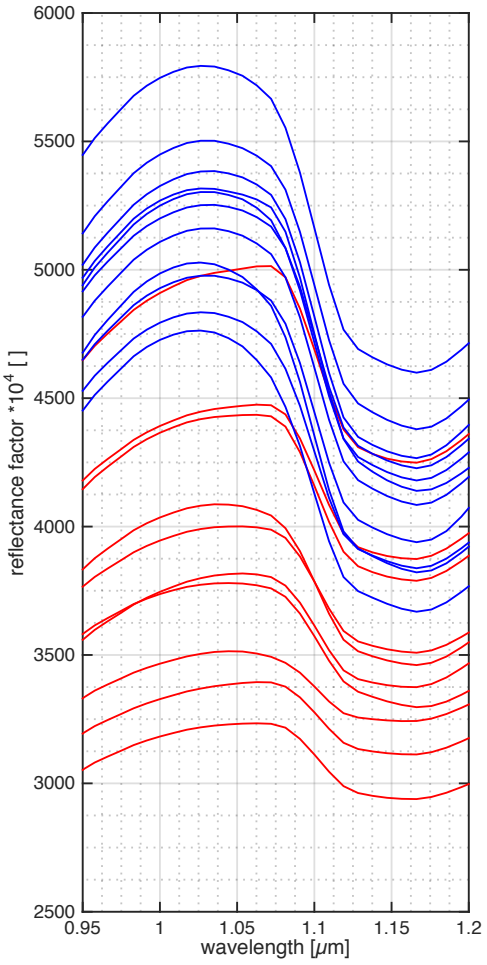

FIGURE 4.5: The spectral shift of about 30 to 40 nm in the near infra red (NIR) at 1.035 μm after applying the general transformation function. ASD' spectra from 06.08.13 are shown in blue and from 12.08.13 in red.

Another possibility to correct the spectral shift would be to define the minima and maxima for each pair of ASD and APEX spectra independently and apply specific spectral shift correction functions. This approach would be possible for spectra showing explicit characteristics where local minima and maxima can clearly be distinguished. The higher the VCR the more distinct the minima and maxima become.

A further possibility could be to perform an inflight calibration in ATCOR to calibrate the APEX image based on the ASD measurements. However, this requires homogeneous data, which were not available in this study due to the differences in the ASD data from cluster 3 and 4 in July (Chapters 4.1.1 and 4.1.2).

4.2 APEX classification and unmixing

The APEX classification revealed an artefact based on two wires placed in the entry slit of APEX (Figure 3.1). As the artefact did not affect any of the plots of this study, no further steps were taken to analyse or eliminate it. However, the artefact was preserved in the transformed APEX images APEX'June and APEX'August.Thus, the pixels in the interpolated wire region have to be treated with caution in all three images.
To validate the classification, ground truth data would have been beneficial. As this study was focused on grassland, no field data of the other types of cover (rocks, forest etc.) were taken. Therefore, no accuracies of the classification could have been determined.
ASD data can be used for the unmixing of vegetation and soil. Therefore, the ASD spectra of pure vegetation and pure soil should have been used as endmembers. Additionally to the already discussed problem of the spectral shift a high variability in the ASD spectra of pure vegetation and pure soil (Figure 4.6) complicated the determination of appropriate endmembers. Various spectra showed outliers, especially in wavelengths larger than 1.8 μm, wherefore these wavelengths were not suitable for the unmixing.
Several unmixings based on ASD data were performed and all of them showed insufficient results. As at that time of the study the differences between ASD and APEX data had not yet been sufficiently analysed and hardly explained, the ASD pure spectra provided no reliable basis for the unmixing. This demonstrates how important the VV is if two different kinds of data are combined.

The validation of the VCR, determined by the Linear Spectral Unmixing (LSU) based on endmembers selected from the APEX image, was significant but showed a leverage effect (Chapter 3.1.2, Figure 3.2). This effect occurred due to the uneven distribution of the reference plots according to their VCR. A more even coverage of the whole extent of VCR could be improved for future sampling design.
The regression model underestimated the modelled VCR what was the result of two different definitions of VCR. The VCR measured in the field considered multiple vegetation layers and therefore, a plot could have had a VCR of more than 100 %. APEX data do not allow the differentiation between different vegetation layers and the sum of all cover ratios of a pixel was defined as 100 %, resulting in a lower percentage of vegetation compared to the one measured in field. As the alpine grasslands in this study did not show

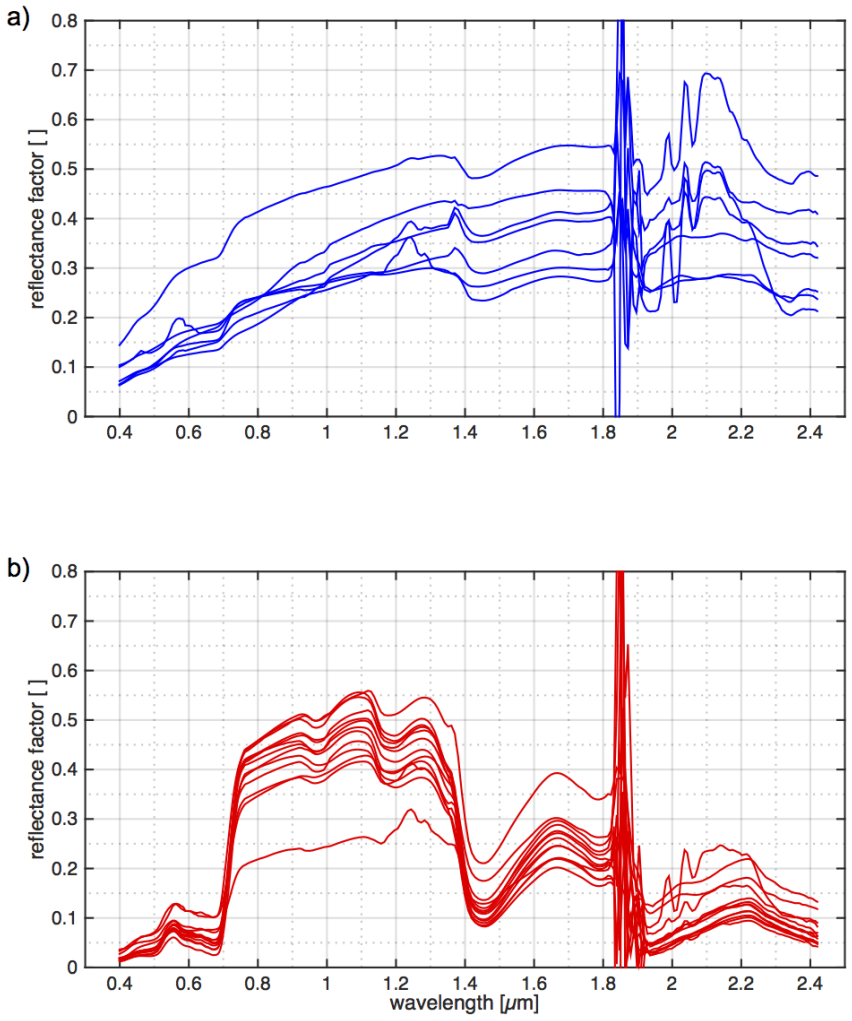

FIGURE 4.6: The ASD spectra of pure soil are shown in blue (a) and the spectra of pure vegetation in red (b).

big differences in their layer structure, the field data based VCR and the airborne data based VCR matched well. But in areas with more complex vegetation structures it could become a problem if field measurements were conducted in another manner compared to the imaging spectrometer data acquisition.

For the VV of the ASD and APEX data and the time transformation of the APEX image all pixels showing less than 40 % VCR were excluded. The reason for this was the lack of ASD data between 25 % and 60 % VCR for the VV and a lack of ASD data below 40 % VCR to determine the time transformation function (TTF). Both problems are discussed in the following Chapters.

4.3 Transformation Vector

The initial target was to determine transformation vectors (TV) for each wavelength, comprising gain and offset to transform the ASD spectra to APEX-like spectra (ASD') after the correction of the spectral shift. The determination and application of the TV was part of the VV. Due to the inconsistencies of the ASD data from July (Chapter 4.1), it was not possible to determine a meaningful gain and offset for each wavelength. Figure 4.7 shows the comparison of ASD and APEX spectra at several wavelengths, coloured by their plot cluster. In many wavelengths the differences in reflectance factors between the cluster 3 plots and the cluster 4 plots, characterised by high VCR, were evident and resulted in negative linear correlations between ASD and APEX for some wavelengths (Figure 4.7d). The yellow line in Figure 4.7 is the overall correlation line on which the initial TV was based on. This TV consisting of gain and offset of the correlations between ASD and APEX lead to unusable results of reflectance factors beneath 0 and above 100 % when being applied to the ASD spectra.

Due to these problems, new TV based on the gain of the ASD and APEX spectra only were determined. Figure 2.6c shows examples of these TV. The differences in reflectance factors of cluster 3 and 4 became also apparent in the corresponding TV.
Additionally, the TV differed much between plots with high and low VCR, respectively (Figure 2.6c). The TV seemed to depend on the VCR, but this assumed dependency could not be further examined due to the lack in ASD data from July between 25 % and 60 % VCR. This lack made it impossible to determine the TV dependent on the VCR for the whole range of the VCR.
Both problems lead to the compromise of using one TV reasonably applicable for as much data as possible. As the value range differences of each pair of ASD and APEX spectra were different and therefore could no be further improved, I determined a TV that adjusted the ASD spectra to the APEX spectra but affected the values as little as possible. This TV was based on the mean ASD and APEX spectra of the cluster 3 plots from July, as there the match between ASD and APEX was the highest. To minimise the change of values, there was a slight adjustment of the TV of 0.84 % to make sure that the sum of reflectance factors (excluding the wavelengths between 1.798 μm and 2.021 μm) stayed the same before and after transformation. This resulted in a slight adjustment of the ASD spectra to the shape of the APEX spectra (Figure 2.6d).

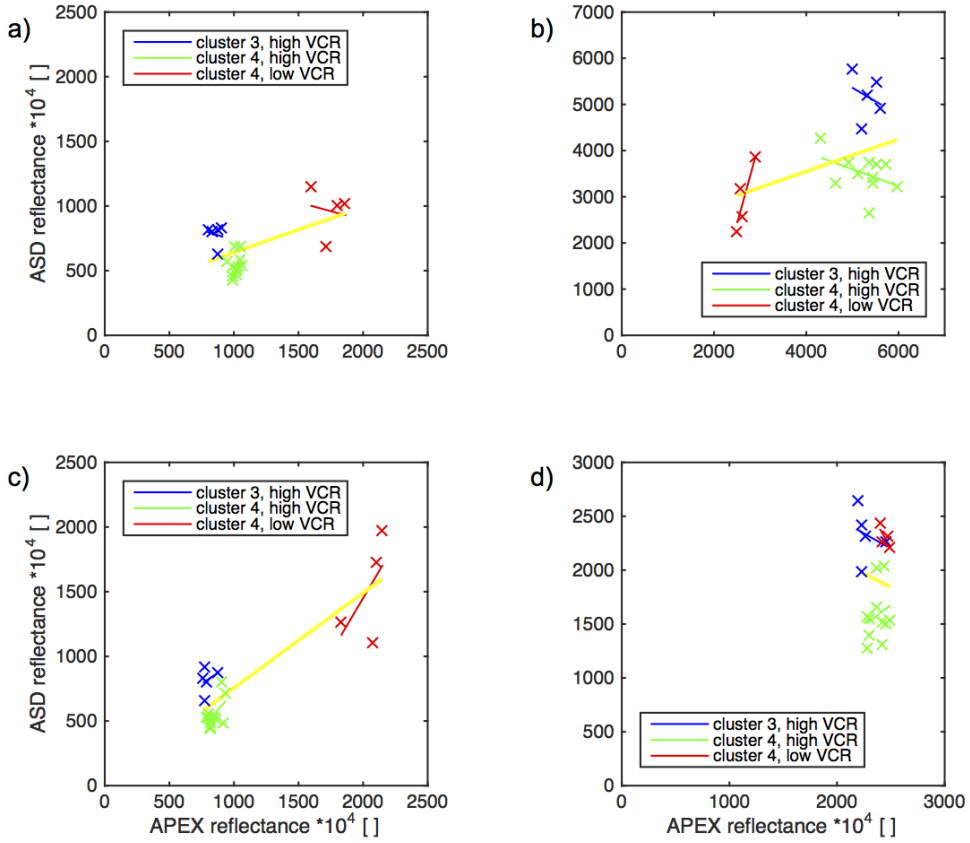

FIGURE 4.7: The comparison of ASD and APEX spectra of July at several wavelengths (a = 0.553 μm, b = 0.844 μm, c = 1.449 μm and d = 1.659 μm), grouped and coloured by their valley segment and their vegetation cover ratio (VCR). The linear correlation of each group is shown in the group's colour and the yellow line is the overall correlation line on which the initial transformation vector (TV) was based on.

This TV produced reasonable results for the plots with VCR between 60 % and 80 % but not for the plots with VCR between 15 % and 25 % (Figure 2.6d). The ASD spectra from June and August, that had to be transformed by the TV, showed a range of 40 % to 85 % VCR, a larger range of VCR than the TV was based on. There was no other possibility than applying the TV to all of the spectra even though it cannot be examined if the VCR is appropriate for spectra with VCR below 60 % and above 80 %. As shown in the ASD spectra from July, there is an influence of the VCR on the TV which could have been examined in more detail if the plots had been more evenly distributed over the whole range of VCR and if the same plots for all three months were sampled. For future studies the distribution of the plots and the sampling regime could be improved to render an investigation of the TV's dependency on the VCR possible. Additionally, the TV could have been affected by other influences, such as recording time or sun and sensor incident angles.

4.4 Time Transformation Function

I concentrate on the creation and application of the time transformation function (TTF) based on the transformation of the APEX image from July to August. Based on the same reasons as for the TV, no meaningful TTF consisting of gain and offset could be developed. Therefore, the gain between the transformed APEX-like ASD spectra (ASD') from August and the APEX spectra from July of each plot was determined as the initial plot specific TTF. Figure 2.7 shows all TTF of August coloured by their VCR.

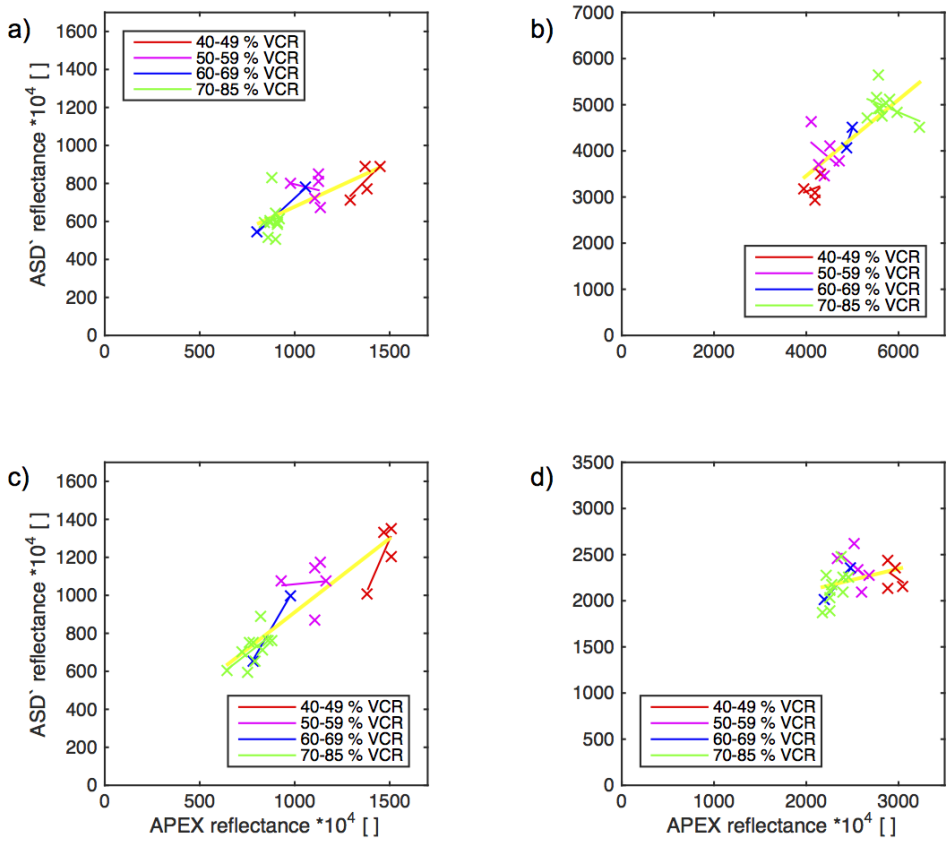

FIGURE 4.8: The comparison of ASD' from August and APEX spectra from July at several wavelengths (a = 0.553 μm, b = 0.844 μm, c = 1.449 μm and d = 1.659 μm), coloured by their vegetation cover ratio (VCR). The linear correlation of each VCR class is shown in the corresponding colour and the yellow line is the overall correlation line on which the initial time transformation function (TTF) was based on.

Figure 4.8 shows the comparison of the ASD'August and the APEX spectra from July of each plot coloured by their VCR. In contrast to July, dependencies on the VCR in both data sets and several wavelengths can be observed. Different analyses concerning the dependency of TTF and VCR have been performed. Figure 4.9 shows one of these results where mean TTF for 5 % steps of VCR between 50 % and 85 % have been

calculated. Figure 4.9 shows the TTF for all 284 bands split into 4 parts: visible, NIR and SWIR before and after the cut wavelengths. Initially, it was expected that the TTF depends on VCR as only the vegetation, but not the soil, changes within the months. The higher the VCR the bigger change in reflectance factors was expected. As vegetation changes can best be recognised in the NIR, hence I focused on these wavelengths (Figure 4.9b). The reflectance factors declined from July to August for nearly all plots. If not in dependency from VCR, the TTFs of all bands would be horizontally orientated. If the reflectance factors of plots with higher VCR changed more, the TTF would incline from the upper left to the lower right corner. This was the case between 60 % and 80 % VCR, but not for lower VCR. The TTF of plots with low and with high vegetation cover fraction behave similar, but differently to the TTF of plots with medium VCR. This behaviour could not be explained.

Figure 4.10, a 3D surface of the TTF, shows artefacts mainly at the red edge and after the excluded water vapour absorption bands. These were more distinct for plots with low VCR. The origin of the artefact can be seen in Figure 2.6. All TTF showing the artefact after the excluded wavelengths were plots of the cluster 1, whose ASD measurements were taken at a different date than the one from cluster 2 and 3. These differences between the ASD data from 06.08.13 and 12.08.13 did not stand out before but showed another inconsistency in the ASD data.

As the dependency of the TTF on the VCR is contradictory (Figure 4.9) and artefacts appeared in the VCR dependent TTF (Figure 4.10), it was not possible to determine a meaningful TTF depending on VCR. Therefore, an overall suitable TTF had to be found. Different kinds of overall TTF were created, applied to the APEX image and the results were compared. The results were very similar and the ASD spectra and their TTF could not have been classified to more and less beneficial spectra and TTF. Therefore the mean of the TTF of all 21 plots was selected as the final TTF.
The ASD data from June were even less suitable for the determination of a reasonable TTF for the transformation of the APEX image from July to June. The range of the TTF was higher than in August and the TTF were affected by outliers for which reason the TTF was calculated using the mean of the TTF of all plots as before.
One universal TTF for the whole study area cannot assumed to be representative as alpine valleys are characteristed by differnences in the amount and cover of vegetation, species composition, slope, exposition, nutrient availability and different phenological

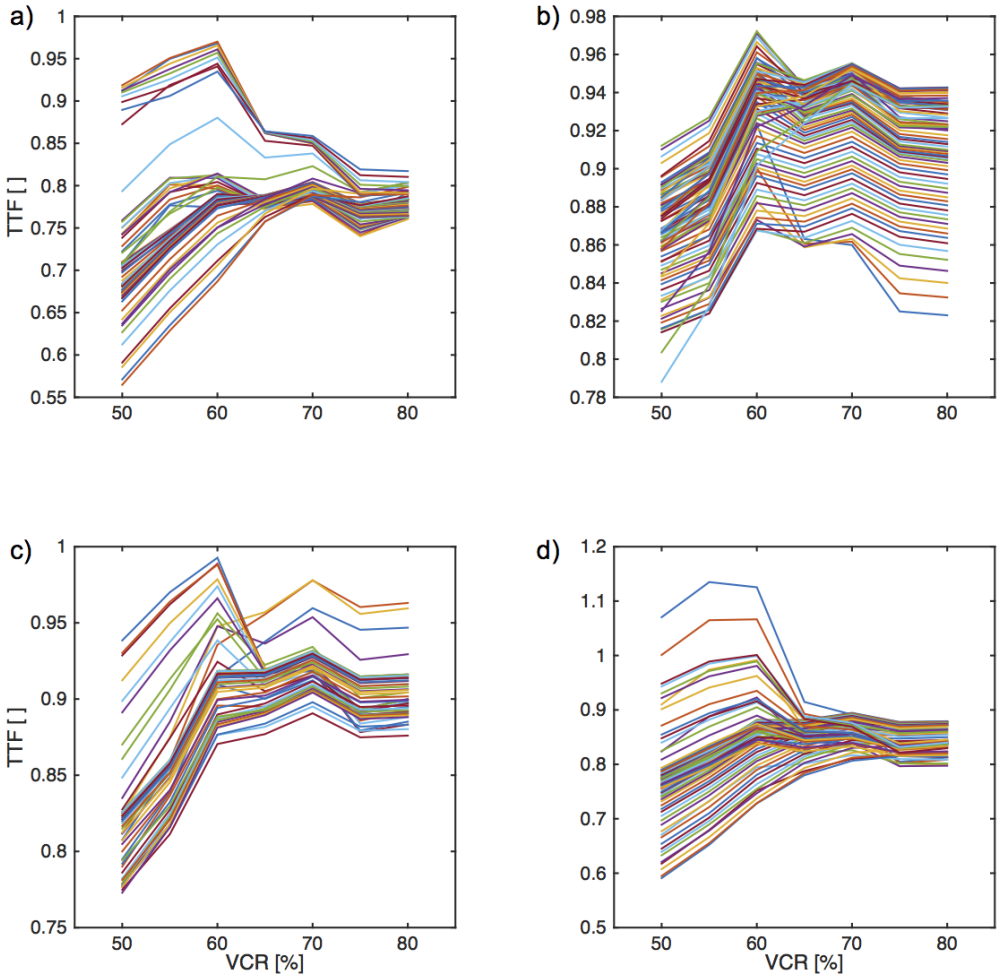

FIGURE 4.9: Cross sections of the time transformation functions (TTF) depending on the vegetation cover ratio (VCR). Each line stands for one band of the 284 APEX bands. Figure a) shows the bands with wavelengths from 0.399 to 0.720 μm (visible), Figure b) from 0.724 to 1.331 μm (near infra red (NIR)), Figure c) from 1.341 to 1.756 μm (short wave infra red (SWIR)) and Figure d) from 1.936 to 2.420 μm (SWIR).

stages that affect the development of alpine grasslands within one month.

At the beginning of the study it was planned to recompose the synthetic APEX images. However, as sparsely vegetated alpine grassland (VCR $<$ 40 %) could not be reasonably transformed, a recomposition of unchanged and transformed pixels was not possible.

4.5 Biomass models

For validation of the synthetic APEX images (APEX'), biomass was derived from spectral measurements, wherefore spectral indices are suitable. One of the most used spectral indices, the NDVI, was chosen. As the NDVI saturates with high biomass and high

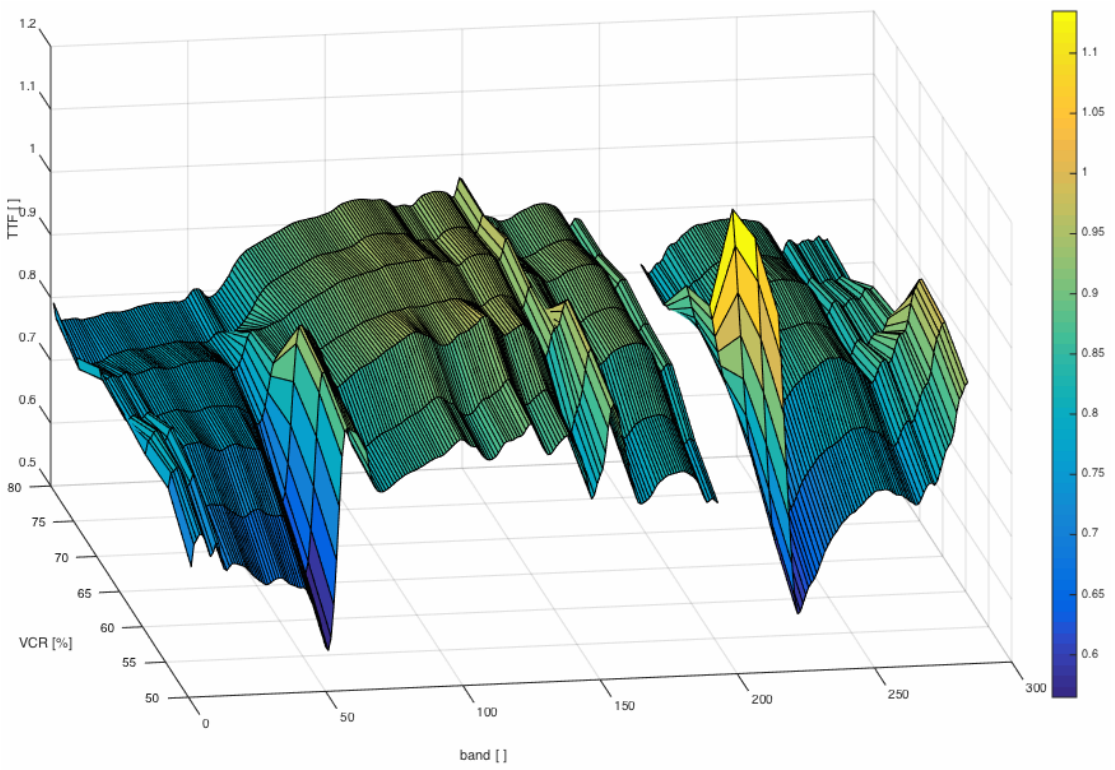

FIGURE 4.10: 3D surface of the time transformation function (TTF) for all bands depending on the vegetation cover ratio (VCR).

Leaf Area Index (LAI, Chen et al. (1991)), the Enhanced Vegetation Index (EVI, Liu and Huete (1995)) may be a better alternative (e.g. Huete et al. (1997); Guo et al. (2007); Wang et al. (2005)). For the whole test site, NDVI and LAI were calculated and compared and no saturation of the NDVI in areas with high LAI was observed; consequently, the NDVI was chosen to build the biomass models.

For the calculation of the NDVI, the red minimum at 0.675 μm (band 51) and the first NIR maximum at 0.844 μm (band 90) were chosen. To test the sensitivity of the NDVI to band selection, NDVI values based on several band combinations of $\pm$ 5 bands (about $\pm$ 30 nm) were calculated and compared. The NDVI differed only marginally, thus the NDVI can be assumend to be stable and not affected by possible residual spectral shifts. The wavelengths of the red minimum and the first NIR maximum of other spectral data could differ and therefore have to be identified separately for each data set separately.

As the R^2 of the models of ASD and ASD' differed negligibly (largest difference 0.01), the transformation from ASD to ASD' did only minimally change the values, as it was intended.

The cross validation (CV; Diaconis and Efron (1983)) of the original APEX image showed

the quality of the model based on NDVI and biomass, that was quite low (R^2 = 0.27, Figure 3.6). The split of the biomass data and performance of Leave One Out Cross Validations (LOO-CV; Cawley and Talbot (2004)) based on 19 and 21 measurements showed big differences (R^2 of 0.82 and -0.10, Figure 3.7). These results demonstrate that the performance of the chosen exponential model based on the same data set (APEX July) differs much, depending on which biomass measurements were selected for the model. As the quality of the model can be influenced that easily, the model appears not to be stable.

The results of the 8 performed models do not allow drawing conclusions if ASD or APEX data was more suitable for biomass predictions. For all but one model, the chosen exponential correlation between NDVI and biomass was appropriate. As the creation of biomass models was not the main issue but only a validation tool in this study, the models are not further discussed. For more information about biomass models of alpine grassland in the SNP, especially Val Trupchun, see Schweiger et al. (2014) and Schweiger et al. (2015).

As mentioned in the last Chapter, several other time transformed APEX images from August were calculated based on different TTF and were validated following the same procedure as for APEX'August. All of them showed exactly the same result (R^2 = 0.56), wherefore this validation method was not suited to detect any differences in the overall performance of the chosen TTF compared to other possible TTF.

To correlate single absorption bands with the nitrogen or leaf water content (e.g. Dury and Turner (2001), Clevers and Kooistra (2009)) was not possible due to uncertain positions of the absorption bands as a result of the atmospheric compensation problems and the spectral shifting during the VV.

4.6 Discussion of the hypotheses

The goal of this master thesis was to create two synthetic APEX images based on one APEX image and ASD measurements from three different months. Based on this goal four hypotheses had been formulated that are discussed in the following paragraphs.

I. The cover ratio of vegetation and soil of the alpine grassland can be determined using Linear Spectral Unmixing (LSU).

The vegetation cover ratio (VCR) was successfully determined using LSU based on two endmembers within the APEX image (Chapter 4.2). However, it was not possible to use the ASD measurements of pure vegetation and pure soil as endmembers, due to the atmospheric compensation problems. These had led to wrong vapour estimation in ATCOR and consequently to wrong features in the APEX reflectance spectra.
As the validation approved the VCR, this first hypothesis can be confirmed, although it is necessary to pay attention to the definitions of VCR when measured in the field and when derived from imaging spectrometer data.

II. For each wavelength a transformation vector (TV) consisting of a proportional linear gain and a proportional offset can be identified to transform ASD spectra to APEX equivalent spectra or vice versa.

As discussed in Chapter 4.3 it was not possible to develop a TV consisting of linear gain and offset due to, partly unexplained, inconsistencies in the ASD data. The chosen solution with a TV only based on the offset between several ASD spectra and the corresponding APEX spectra seems appropriate, but has some restrictions. The TV depends on the VCR of a pixel but could not be modelled in dependence of the VCR. The TV is built for pixels with 60 % to 80 % VCR and is appropriate for this VCR range. However, it's suitability when applied to pixels with 40 % to 60% VCR and 80 % to 100 % VCR could not be tested.
The TV is applicable to transform ASD spectra to APEX like spectra and vice versa.
Half of the hypothesis has to be rejected, half can be confirmed as a TV could be identified but it is only based on gain and not on gain and offset.

III. The change in spectral behaviour over time is proportional to the vegetation cover ratio.

There are indications that the spectral behaviour over time, and hence also the TTF, depends on the VCR (Chapter 4.4). The found dependencies are not conclusive and an overall TFF independent on the VCR had to be determined. Therefore this hypothesis can neither be confirmed nor rejected.

IV. The combination of airborne and ground based spectral data allows creating synthetic spectral time series.

The combination of these two kinds of data from common and different measurement dates and times can be used to build synthetic time series. Two synthetic spectral images were created in this study, nevertheless the main goal of this study was not satisfactorily achieved. The major reason accounting for this issue is the inconstancy of the data, caused by an inconsistent sampling regime and large variations and uncertainties in the data. A more consistent and controlled data basis would lead to more possibilities to evaluate the data and find explanations for occurring irregularities and relationships. Since the quality of the two synthetic images cannot be sufficiently determined, they have to be used with caution.

Chapter 5

Conclusion & Outlook

This master thesis was an explorative study that combined ground based spectral measurements and airborne imaging spectrometer data to create a synthetic time series. The focus was laid on the correlation strength between airborne and ground based data acquisitions. Compared to other studies, where ground based and airborne or satellite based data were combined (e.g. Boschetti et al. (2007); Psomas et al. (2007); Numata et al. (2008)), preprocessing steps of the data set in this study exceeded simple convolutions before combining the data. The conducted vicarious validation (VV) disclosed many problems as atmospheric compensation problems for the APEX data, differences in the ASD reflectance factors between clusters and measurements dates, outliers in the ASD data and high scattering in the white reference measurements.

Based on gaps in the data basis a large part of the study area had to be excluded and more data would been beneficial for better understanding of the data, its differences and its relations. If the transformation vector (TV) and the time transformation function (TTF) shall be determined dependent on vegetation cover ratio (VCR) or on other variables, higher sample numbers and more broadly based data would be required. The study area was large and heterogeneous and typically for an alpine valley, there are differences in the amount of vegetation, species, slope, exposition and nutrient availability that affect the development of alpine grasslands during the course of the grwoing season. Therefore, one universal TV and TTF for the whole study area is not representative.

Generally, the TTF as time transformation can strengthen or reduce existing features in the data but hardly add new characteristics. Therefore, it is recommended to use the time transformation approach of this study only for time transformations of short

time spans where similar behaviour of the vegetation within the whole study area can be expected.

The atmospheric compensation problems in the processing of the APEX data rose the differences between ASD and APEX data. However, based on the experience of this study it must be strongly recommended to analyse and compare the different kinds of data in detail before combining it.

As the validation of the two synthetic APEX images could not be performed in sufficient detail, they have to be used with caution. However, they can be used to examine the behaviour of vegetation parameters over time or to determine the vegetation peak for example. This synthetic time series can be used for well established applications, as the NDVI is, but not for the development of new analysis methods or for analyses based on marginal differences in the reflectance factors or specific wavelengths and the accuracy of the results has always to be considered carefully.

Synthetic time transformations, as performed in this thesis, are strongly sensor and site specific. If time transformations shall be done based on ASD and APEX data of a different year or location than in this study, the data has to be examined individually and accurately anew.

A better result could be achieved in a less heterogeneous study area. However, the data basis is crucial for a successful time transformation. The sampling design has to be well elaborated, contain more plots than this study and cover the entire range of vegetation types and possible influence factors on the vegetation development in the study area. For all points in time the same measurements (ASD spectra, biomass, photo) shall be taken and in the same way. Although the huge variantion in the WR spectra in this study cannot be explained, it is recommended to limit the measurements to a closer time range. Additionally, the availability of reference data for a meaningful validation is mandatory.

Another approach to create synthetic time series could be to simulate the vegetation development based on site factors, such as nutrient and water availability, amount of vegetation, species composition or exposition. As combination of both models, the nitrogen or water availability (preferably the limiting growth factors for a given environment) can be determined based on the APEX image and combined with the TTF based on the ASD data. As vegetation growth depends on a large number of factors, the challenge of future studies will be to find the most influential ones for the corresponding study area and develop models to approximate to the natural vegetation development.

Bibliography

Boschetti, M., Bocchi, S., and Brivio, P. A. (2007). Assessment of pasture production in the Italian Alps using spectrometric and remote sensing information. *Agriculture, Ecosystems and Environment*, 118:267–272.

Bryant, R., Moran, M., McElroy, S., Holifield, C., Thome, K., and Miura, T. (2002). Data continuity of Landsat-4 TM, Landsat-5 TM, Landsat-7 ETM+, and Advanced Land Imager (ALI) sensors. *IEEE International Geoscience and Remote Sensing Symposium*, 1:584–586.

Cawley, G. C. and Talbot, N. L. C. (2004). Fast exact leave-one-out cross-validation of sparse least-squares support vector machines. *Neural networks : the official journal of the International Neural Network Society*, 17(10):1467–75.

Chen, J., Black, T., and Adams, R. (1991). Evaluation of hemispherical photography for determining plant area index and geometry of a forest stand. *Agricultural and Forest Meteorology*, 56(1-2):129–143.

Chen, J., Gu, S., Shen, M., Tang, Y., and Matsushita, B. (2009). Estimating aboveground biomass of grassland having a high canopy cover: an exploratory analysis of in situ hyperspectral data. *International Journal of Remote Sensing*, 30(24):6497–6517.

Clevers, J. and Kooistra, L. (2009). Using hyperspectral remote sensing data for retrieving canopy water content. *First Workshop on Hyperspectral Image and Signal Processing: Evolution in Remote Sensing, Grenoble, France*, pages 2–5.

Damm, A., Guanter, L., Verhoef, W., Schläpfer, D., Garbari, S., and Schaepman, M. E. (2015). Impact of varying irradiance on vegetation indices and chlorophyll fl uorescence derived from spectroscopy data. *Remote Sensing of Environment*, 156:202–215.

Damm, A., Kneubuhler, M., Schaepman, M. E., and Rascher, U. (2012). Evaluation of gross primary production (GPP) variability over several ecosystems in Switzerland using sun-induced chlorophyll fluorescence derived from APEX data. *International Geoscience and Remote Sensing Symposium (IGARSS), Munich, Germany*, pages 7133–7136.

Demircan, A. and Mauser, W. (1994). Yield estimation for corn with multitemporal and multisensoral remote sensing data. *Geoscience and Remote Sensing Symposium, 1994. IGARSS '94. Surface and Atmospheric Remote Sensing: Technologies, Data Analysis and Interpretation*, 2:832 – 834.

Diaconis, P. and Efron, B. (1983). Computer intensive methods in statistics. *Scientific American*, 248(5):115–130.

Dury, S. and Turner, B. (2001). Nutrient estimation of eucalypt foliage derived from hyperspectral data. *Geoscience and Remote Sensing Symposium, 2001. IGARSS '01. IEEE 2001 International, Sydney, NSW*, 2:774–776.

Esch, T., Metz, a., Marconcini, M., and Keil, M. (2014). Combined use of multi-seasonal high and medium resolution satellite imagery for parcel-related mapping of cropland and grassland. *International Journal of Applied Earth Observation and Geoinformation*, 28:230–237.

Gao, B. C. (1996). NDWI - A normalized difference water index for remote sensing of vegetation liquid water from space. *Remote Sensing of Environment*, 58(3):257–266.

Gege, P., Fries, J., Haschberger, P., Schötz, P., Schwarzer, H., Strobl, P., Suhr, B., Ulbrich, G., and Vreeling, W. J. (2009). Calibration facility for airborne imaging spectrometers. *ISPRS Journal of Photogrammetry and Remote Sensing*, 64(4):387–397.

Guo, N., Wang, X., Cai, D., and Yang, J. (2007). Comparison and evaluation between MODIS vegetation indices in Northwest China. *International Geoscience and Remote Sensing Symposium (IGARSS), Barcelona, Spain*, pages 3366–3369.

Hardisky, M., Klemas, V., and Smart, R. (1983). The influence of soil salinity, growth form, and leaf moisture on spectral radiance of spartina alterniflora canopies. *Photogrammetric Engineering and Remote Sensing*, pages 77–83.

Hueni, A., Biesemans, J., Meuleman, K., Dell'Endice, F., Schlapfer, D., Odermatt, D., Kneubuehler, M., Adriaensen, S., Kempenaers, S., Nieke, J., and Itten, K. I. (2009a). Structure, components, and interfaces of the airborne prism experiment (APEX) processing and archiving facility. *IEEE Transactions on Geoscience and Remote Sensing*, 47(1):29–43.

Hueni, A., Lenhard, K., Baumgartner, A., and Schaepman, M. E. (2013a). Airborne Prism Experiment Calibration Information System. *IEEE Transactions on Geoscience and Remote Sensing*, 51(11):5169–5180.

Hueni, A., Nieke, J., Schopfer, J., Kneubühler, M., and Itten, K. (2009b). The spectral database SPECCHIO for improved long-term usability and data sharing. *Computers & Geosciences*, 35(3):557–565.

Hueni, A., Sterckx, S., and Jehle, M. (2013b). Operational calibration of APEX. *2013 IEEE International Geoscience and Remote Sensing Symposium - IGARSS*, pages 4423–4426.

Hueni, A., Sterckx, S., Jehle, M., D'Odorico, P., Vreys, K., Bomans, B., Biesemans, J., Meuleman, K., and Schaepman, M. (2012). Operational status of apex and characteristics of the apex open science data set. *2012 IEEE International Geoscience and Remote Sensing Symposium*, pages 5009–5012.

Huete, A. R. (1988). A soil adjusted vegetation index savi. *Remote Sensing of Environment*, 25:295–309.

Huete, A. R., Liu, H. L. H., and Leeuwen, W. V. (1997). The use of vegetation indices in forested regions: issues of linearity and saturation. *IGARSS'97. 1997 IEEE International Geoscience and Remote Sensing Symposium Proceedings. Remote Sensing - A Scientific Vision for Sustainable Development*, 4(1):1966–1968.

Jehle, M., Hueni, A., Damm, A., D'Odorico, P., Weyermann, J., Kneubühler, M., Schläpfer, D., Schaepman, M. E., and Meuleman, K. (2010). APEX - Current status, performance and validation concept. *In: Proceedings IEEE Sensors, Hawaii, US*, pages 533–537.

Kerr, J. T. and Ostrovsky, M. (2003). From space to species: Ecological applications for remote sensing. *Trends in Ecology and Evolution*, 18(6):299–305.

Kneubuehler, M., Schaepman, M. E., and Kellenberger, T. W. (1998). Comparison of Different Approaches of Selecting Endmembers to Classify Agricultural Land by Means of Hyperspectral Data (DAIS7915). *IGARSS 1998*, pages 888–890.

Kneubühler, M., Damm, A., Schweiger, A.-K., Risch, A. C., Schütz, M., and Schaepman, M. E. (2014). Continuous Fields From Imaging Spectrometer Data for Ecosystem Parameter Mapping and Their Potential for Animal Habitat Assessment in Alpine Regions. *IEEE Journal of Selected Topics in Applied Earth Observations and Remote Sensing*, 7(6):2600–2610.

Kneubühler, M., Schaepman, M. E., and Thome, K. J. (2003). MERIS/ENVISAT first year vicarious calibration results from Railroad Valley Playa (NV). *Envisat MAVT-2003 - Working meeting on MERIS and AATSR Calibration and Geophysical Validation.*

Kokaly, R. F., Despain, D. G., Clark, R. N., and Livo, K. E. (2007). Spectral Analysis of Absorption Features for Mapping Vegetation Cover and Microbial Communities in Yellowstone National Park Using AVIRIS Data. *Publications of the US Geological Survey.*

Lawley, V., Lewis, M., Clarke, K., and Ostendorf, B. (2015). Site-based and remote sensing methods for monitoring indicators of vegetation condition: An Australian review. *Ecological Indicators*, In Press.

Li, X., Ge, L., Cholathat, R., and Hu, Z. (2013a). Innovative NDVI time-series analysis based on multispectral images for detecting small scale vegetation cover change. *Geoscience and Remote Sensing Symposium (IGARSS), 2013 IEEE International, Melbourne, VIC*, pages 4297–4300.

Li, Z., Huffman, T., McConkey, B., and Townley-Smith, L. (2013b). Monitoring and modeling spatial and temporal patterns of grassland dynamics using time-series MODIS NDVI with climate and stocking data. *Remote Sensing of Environment*, 138:232–244.

Liu, H. Q. and Huete, A. (1995). Feedback based modification of the NDVI to minimize canopy background and atmospheric noise. *IEEE Transactions on Geoscience and Remote Sensing*, 33(2):457–465.

Lymburner, L., McIntyre, A., Fuqin L. amd Ip, A., Thankappan, M., and Sixsmith, J. (2013). Creating multi-sensor time series using data from Landsat-5 TM and Landsat-7

ETM+ to characterise vegetation dynamics. *Geoscience and Remote Sensing Symposium (IGARSS), 2013 IEEE International, Melbourne, VIC*, pages 961 – 963.

Muchoney, D. M. (2008). Earth observations for terrestrial biodiversity and ecosystems. *Remote Sensing of Environment*, 112(5):1909–1911.

Mutanga, O., Skidmore, A. K., and Prins, H. H. T. (2004). Predicting in situ pasture quality in the Kruger National Park, South Africa, using continuum-removed absorption features. *Remote Sensing of Environment*, 89:393–408.

Numata, I., Roberts, D. a., Chadwick, O. a., Schimel, J. P., Galvão, L. S., and Soares, J. a. V. (2008). Evaluation of hyperspectral data for pasture estimate in the Brazilian Amazon using field and imaging spectrometers. *Remote Sensing of Environment*, 112:1569–1583.

Pottier, J., Malenovský, Z., Psomas, A., Homolová, L., Schaepman, M. E., Choler, P., Thuiller, W., Guisan, A., and Zimmermann, N. E. (2014). Modelling plant species distribution in alpine grasslands using airborne imaging spectroscopy. *Biology letters*, 10(7).

Psomas, A., Itten, K., and Zimmermann, N. E. (2007). Hyperspectral remote sensing for seasonal estimation of aboveground biomass in Swiss grassland habitats. *ISPRS Working Group VII/1 Workshop ISPMSRS'07: Physical Measurements and Signatures in Remote Sensing*.

Pullanagari, R. R., Yule, I. J., Tuohy, M. P., Hedley, M. J., Dynes, R. a., and King, W. M. (2011). In-field hyperspectral proximal sensing for estimating quality parameters of mixed pasture. *Precision Agriculture*, 13(3):351–369.

Rahman, A. F. and Gamon, J. a. (2004). Detecting biophysical properties of a semi-arid grassland and distinguishing burned from unburned areas with hyperspectral reflectance. *Journal of Arid Environments*, 58:597–610.

Ramoelo, A., Skidmore, a. K., Cho, M. a., Mathieu, R., Heitkönig, I. M. a., Dudeni-Tlhone, N., Schlerf, M., and Prins, H. H. T. (2013). Non-linear partial least square regression increases the estimation accuracy of grass nitrogen and phosphorus using in situ hyperspectral and environmental data. *ISPRS Journal of Photogrammetry and Remote Sensing*, 82:27–40.

Richter, R. and Schläpfer, D. (2002). Geo-atmospheric processing of airborne imaging spectrometry data. Part 2: Atmospheric/topographic correction. *International Journal of Remote Sensing*, 23:2631–2649.

Richter, R., Schläpfer, D., and Müller, A. (2011). Operational atmospheric correction for imaging spectrometers accounting for the smile effect. *IEEE Transactions on Geoscience and Remote Sensing*, 49(5):1772–1780.

Rouse, J., Haas, R., and Schell, J. (1974). Monitoring the vernal advancement and retrogradation (greenwave effect) of natural vegetation. *Texas A & M University*, pages 1–8.

Schaepman, M. E., Jehle, M., Hueni, A., D'Odorico, P., Damm, A., Weyermann, J., Schneider, F. D., Laurent, V., Popp, C., Seidel, F. C., Lenhard, K., Gege, P., Küchler, C., Brazile, J., Kohler, P., De Vos, L., Meuleman, K., Meynart, R., Schläpfer, D., Kneubühler, M., and Itten, K. I. (2015). Advanced radiometry measurements and Earth science applications with the Airborne Prism Experiment (APEX). *Remote Sensing of Environment*, 158:207–219.

Schläpfer, D. and Richter, R. (2002). Geo-atmospheric processing of airborne imaging spectrometry data. Part 1: Parametric orthorectification. *International Journal of Remote Sensing*, 23:2609–2630.

Schuster, C., Schmidt, T., Conrad, C., Kleinschmit, B., and Förster, M. (2015). Grassland habitat mapping by intra-annual time series analysis - Comparison of RapidEye and TerraSAR-X satellite data. *International Journal of Applied Earth Observation and Geoinformation*, 34:25–34.

Schweiger, A. K., Risch, A. C., Damm, A., Kneubühler, M., Haller, R., Schaepman, M. E., and Schütz, M. (2014). Using imaging spectroscopy to predict above ground plant biomass in alpine grasslands grazed by large ungulates. *Journal of Vegetation Science*, 26(1):175–190.

Schweiger, A. K., Schütz, M., Anderwald, P., Schaepman, M. E., Haller, R., and Risch, A. C. (2015). Foraging ecology of three sympatric ungulate species – Behaviour and resource maps indicate differences between chamois , ibex and red deer. *Movement Ecology*, accepted.

Sha, Z., Brown, D. G., and Welsh, W. F. (2012). Discriminating Stocking Rates in a Typical Grassland Using in situ Spectral Reflectance Data. *Earth Observation and Remote Sensing Applications (EORSA), 2012 Second International Workshop, Shanghai, China*, pages 120 – 124.

Small, C. and Lu, J. W. (2006). Estimation and vicarious validation of urban vegetation abundance by spectral mixture analysis. *Remote Sensing of Environment*, 100(4):441–456.

Tucker, C. J. (1979). Red and photographic infrared linear combinations for monitoring vegetation. *Remote Sensing of Environment*, 8(2):127–150.

Vescovo, L. and Gianelle, D. (2008). Using the MIR bands in vegetation indices for the estimation of grassland biophysical parameters from satellite remote sensing in the Alps region of Trentino (Italy). *Advances in Space Research*, 41(11):1764–1772.

Wang, Q., Adiku, S., Tenhunen, J., and Granier, A. (2005). On the relationship of NDVI with leaf area index in a deciduous forest site. *Remote Sensing of Environment*, 94(2):244–255.

Personal Declaration

I hereby declare that the submitted thesis is the result of my own, independent work. All external sources are explicitly acknowledged in this thesis.

_____ _____

Place, Date Signature